Review

Isospin-Symmetry Breaking within the Nuclear Shell Model: Present Status and Developments

Nadezda A. Smirnova

Laboratoire de Physique des Deux Infinis Bordeaux (LP2IB), Centre National de la Recherche Scientifique, Institut National de Physique Nucléaire et de Physique des Particules (CNRS/IN2P3), Université de Bordeaux, 33175 Gradignan, France; nadezda.smirnova@u-bordeaux.fr

Abstract: The paper reviews the recent progress in the description of isospin-symmetry breaking within the nuclear shell model and applications to actual problems related to the structure and decay of exotic neutron-deficient nuclei and nuclei along the $N = Z$ line, where N is the neutron number and Z the atomic number. The review recalls the fundamentals of the isospin formalism for two-nucleon and many-nucleon systems, including quantum numbers, the spectrum's structure and selection rules for weak and electromagnetic transitions; and at the end, summarizes experimental signatures of isospin-symmetry breaking effects, which motivated efforts towards the creation of a relevant theoretical framework to describe those phenomena. The main approaches to construct accurate isospin-nonconserving Hamiltonians within the shell model are briefly described and recent advances in the description of the structure and (isospin-forbidden) decay modes of neutron-deficient nuclei are highlighted. The paper reviews major implications of the developed theoretical tools to (i) the fundamental interaction studies on nuclear decays and (ii) the estimation of the rates of nuclear reactions that are important for nuclear astrophysics. The shell model is shown to be one of the most suitable approaches to describing isospin-symmetry breaking in nuclear states at low energies. Further efforts in extending and refining the description to larger model spaces, and in developing first-principle theories to deal with isospin-symmetry breaking in many-nucleon systems, seem to be indispensable steps towards our better understanding of nuclear properties in the precision era.

Keywords: nuclear shell model; isospin symmetry and its breaking; structure of neutron-deficient nuclei; superallowed Fermi beta decay; fundamental interactions; astrophysical rp-process

1. Introduction

1.1. Isospin Symmetry in Nuclear Structure

Atomic nuclei are unique quantum many-body systems composed of two sorts of fermions—protons and neutrons, which are known to have similar masses and possess similar properties with respect to the strong interactions. It was Heisenberg [1] (see English translation in Ref. [2]) who soon after the discovery of the neutron, introduced an *isospin formalism* similar to the ordinary spin formalism as an elegant mathematical tool for dealing with protons and neutrons. Nucleons are considered to be isospin $t = 1/2$ particles and represented by two-component spinors spanning an abstract vector space where the isospin operator, $\hat{\mathbf{t}}$, acts. The neutron and the proton are two eigenstates of $\hat{t}_3$ (the third component of the isospin operator):

$$\psi_n(\vec{r}) = \psi(\vec{r})\begin{pmatrix} 1 \\ 0 \end{pmatrix}, \ \psi_p(\vec{r}) = \psi(\vec{r})\begin{pmatrix} 0 \\ 1 \end{pmatrix},$$

with eigenvalues $m_t = \pm 1/2$, respectively, and $\vec{r}$ the radius vector. The three components of the isospin operator, analogues of the Cartesian components, generate an isospin SU(2) algebra:

$$[\hat{t}_j, \hat{t}_k] = i\epsilon_{jkl}\hat{t}_l, \tag{1}$$

where $j, k, l = 1, 2, 3$, ϵ_{jkl} is the Levi-Civita symbol, and the square of the isospin operator,

$$\hat{\mathbf{t}}^2 = \hat{t}_1^2 + \hat{t}_2^2 + \hat{t}_3^2 , \tag{2}$$

commutes with each of the components: $[\hat{\mathbf{t}}^2, \hat{t}_j] = 0$.

Operators corresponding to various physical observables can be conveniently expressed using isospin formalism. For example, the third component of the isospin operator $\hat{t}_3$ allows one to express the nucleon charge operator,

$$\hat{q} = \left(\frac{1}{2} - \hat{t}_3 \right) e ,$$

and the ladder operators $\hat{t}_\pm$,

$$\hat{t}_\pm = \hat{t}_1 \pm i\hat{t}_2 , \tag{3}$$

transforming a proton into a neutron and vice versa, can be useful to formulate nuclear β decay. Here, "e" denotes the elementary charge.

Nowadays, isospin symmetry is an important concept in particle physics describing a symmetry between *u* and *d* quarks with respect to the strong interaction and their similarly light masses as compared to the other known quarks. The isospin character of nucleons, and of other hadrons composed from *u* and/or *d* quarks, is a consequence of isospin coupling.

Based on the conservation of charge and the approximate charge-independence of the nuclear forces, Wigner [3] introduced the total isospin operator for an *A*-nucleon system arising from the coupling of the individual isospin operators:

$$\hat{\mathbf{T}} = \sum_{k=1}^{A} \hat{\mathbf{t}}(k) ,$$

or for the components:

$$\hat{T}_\pm = \sum_{k=1}^{A} \hat{t}_\pm(k) , \quad \hat{T}_3 = \sum_{k=1}^{A} \hat{t}_3(k) , \tag{4}$$

with $T(T+1)$ and $M_T = (N-Z)/2$ being eigenvalues of $\hat{\mathbf{T}}^2$ and $\hat{T}_3$, respectively, N the neutron number, and Z the atomic number. A charge-independent nuclear Hamiltonian would commute with $\hat{\mathbf{T}}$,

$$[\hat{H}_{\text{nucl}}, \hat{\mathbf{T}}] = 0 ,$$

or

$$[\hat{H}_{\text{nucl}}, \hat{T}_\pm] = [\hat{H}_{\text{nucl}}, \hat{T}_3] = 0 .$$

An additional isospin quantum number T appears to label *A*-nucleon states besides the total angular momentum, *J*, and parity, π. The spectrum of H_{nucl} thus consists of degenerate isobaric multiplets, which can be labeled by (J^π, T) in nuclei with the same mass number *A* and $M_T = -T, \dots, T$, called isobaric analogue states (IAS).

It was realized long ago that electromagnetic interactions destroy this degeneracy. However, as it was shown by Wigner [4], this leads mainly to dynamical breaking of the isospin SU(2) symmetry. Indeed, the Coulomb interaction between protons, which is the main source of the isospin-symmetry breaking on the nuclear level, can be represented

as a linear combination of an isoscalar ($\hat{V}^{(0)}$), an isovector ($\hat{V}^{(1)}$) and an isotensor ($\hat{V}^{(2)}$) operator:

$$
\hat{V}_{\mathrm{Coul}} = \sum_{i<k}^{A} \left(\frac{1}{2} - \hat{t}_3(i) \right) \left(\frac{1}{2} - \hat{t}_3(k) \right) \frac{\mathrm{e}^2}{|\vec{r}(i) - \vec{r}(k)|}
$$

$$
= \sum_{i<k}^{A} \left\{ \underbrace{\left[\frac{1}{4} + \frac{1}{3}\hat{\mathbf{t}}(i)\hat{\mathbf{t}}(k) \right]}_{V^{(0)}} - \underbrace{\frac{1}{2}(\hat{t}_3(i) + \hat{t}_3(k))}_{V^{(1)}} + \underbrace{\left[\hat{t}_3(i)\hat{t}_3(k) - \frac{1}{3}\hat{\mathbf{t}}(i)\hat{\mathbf{t}}(k) \right]}_{V^{(2)}} \right\} \frac{\mathrm{e}^2}{|\vec{r}(i) - \vec{r}(k)|} . \tag{5}
$$

By estimating the effect of this charge-dependent operator on the isobaric multiplets within the lowest order perturbation theory (due to its expectation value within the states of a given isospin, T) and applying the Wigner–Eckart theorem in the isospace, one gets an expression quadratic in M_T:

$$
\begin{aligned}
\langle \eta T M_T | \hat{V}_{\mathrm{Coul}} | \eta T M_T \rangle &= \frac{(T M_T 00 | T M_T)}{\sqrt{2T+1}} \langle \eta T || \hat{V}^{(0)} || \eta T \rangle \\
&+ \frac{(T M_T 10 | T M_T)}{\sqrt{2T+1}} \langle \eta T || \hat{V}^{(1)} || \eta T \rangle \\
&+ \frac{(T M_T 20 | T M_T)}{\sqrt{2T+1}} \langle \eta T || \hat{V}^{(2)} || \eta T \rangle ,
\end{aligned} \tag{6}
$$

where double bar denotes reduction in the isospin space; $(T M_T \lambda \mu | T M_T)$ are the Clebsch–Gordan coefficients; and η refers to other quantum numbers characterizing an isobaric multiplet: $\eta = (A, J^\pi, \dots)$. By inserting Clebsch–Gordan coefficients, one gets:

$$
\langle \eta T M_T | V_{\mathrm{Coul}} | \eta T M_T \rangle = E^{(0)}(\eta, T) + E^{(1)}(\eta, T) M_T + E^{(2)}(\eta, T) \left[3M_T^2 - T(T+1) \right] , \tag{7}
$$

where $E^{(\lambda)}(\eta, T)$ are related to the reduced in isospace matrix elements of isotensors, as seen from Equation (6). This expression remains valid if leading-order terms of charge-dependent forces of nuclear origin are included, as discussed in Section 1.2. Such a dependence, re-written for nuclear masses, is known as the isobaric-multiplet mass equation (IMME) [4],

$$
\mathcal{M}(\eta, T, M_T) = a(\eta, T) + b(\eta, T) M_T + c(\eta, T) M_T^2 , \tag{8}
$$

with $\mathcal{M}$ being an atomic mass excess. Experimental a, b and c coefficients can be deduced from available data on nuclear masses and spectra of up to about $A = 71$ [5,6].

Interestingly, Equation (8) holds exceptionally well, even for isobaric multiplets with more than three members ($T > 1$). This makes the IMME a powerful tool for predicting the nuclear masses of nuclei along the $N = Z$ line, as illustrated in Section 3. Deviations from the quadratic form are rare and small. They are specifically searched for in experiments, as they can bring important information on the presence of charge-dependent many-body forces or witness strong isospin mixing.

From a group-theoretical point of view [7], Equation (7), or equivalently, Equation (8), expresses a reduction of the isospin SU(2) group to its SO(2) subgroup. The eigenstates of the full Hamiltonian, $\hat{H}_{\mathrm{nucl}} + \hat{V}_{\mathrm{Coul}}$, can still be characterized by the isospin quantum number T, but the $(2T+1)$-fold degeneracy inherent to the isotopic multiplets is now removed. This effect is analogous to a Zeeman splitting of atomic levels in the presence of a magnetic field.

As every symmetry, isospin symmetry proposes a number of selection rules for various transition operators, on the basis of their tensorial character with respect to the SU(2) group in isospace. For example, allowed β-decay, governed by the vector or axial-vector weak

currents, is described by Fermi (F) or Gamow–Teller (GT) operators, respectively. In the impulse approximation, these operators read

$$\hat{O}_F(\beta^\pm) = \sum_{k=1}^A \hat{t}_\pm(k), \quad \hat{O}_{GT}(\beta^\pm) = \sum_{k=1}^A \hat{\sigma}(k)\hat{t}_\pm(k). \tag{9}$$

Both operators are seen to be isovector components. The Fermi operator is a scalar, and the Gamow–Teller operator is a vector in the ordinary spin space ($\hat{\sigma}$ is the Pauli spin operator). The Wigner–Eckart theorem establishes angular momentum parity, and isospin selection rules can be established for transitions between an initial state ($J_i^{\pi_i}, T_i$) and a final state ($J_f^{\pi_f}, T_f$). For Fermi transitions, one has:

$$\Delta J = 0, \, \Delta T = 0, \, \Delta \pi = 0,$$

and for Gamow–Teller transitions, one has:

$$\Delta J = 0, 1, \, \Delta T = 0, 1, \, \Delta \pi = 0$$
$$(\text{no } J_i = 0 \to J_f = 0).$$

From this one can conclude that $J_i = 0 \to J_f = 0$ decay can be only by the Fermi type.

A similar analysis can be performed for electromagnetic operators. Assuming a one-body structure of nucleonic convection and spin currents and point-like nucleons, electromagnetic operators can be shown to be a linear combination of an isoscalar and an isovector operator [8], e.g., for an operator of multipolarity L, one has $\hat{O}_{LM} = \hat{O}_{LM}^{(0)} + \hat{O}_{LM}^{(1)}$, where $M = -L, \ldots, L$. Therefore, their matrix elements between states of given isospin can be expressed as

$$\langle J_f M_f; T_f M_T | \hat{O}_{LM} | J_i M_i; T_i M_T \rangle = \delta_{T_i T_f} \langle J_f M_f | \hat{O}_{LM}^{(0)} | J_i M_i \rangle$$
$$+ \frac{(T_i M_T 1 0 | T_f M_T)}{\sqrt{2T_f + 1}} \langle J_f M_f; T_f || \hat{O}_{LM}^{(1)} || J_i M_i; T_i \rangle, \tag{10}$$

where $\delta_{T_i T_f}$ is the Kronecker delta.

From Equation (10) one immediately gets the isospin selection rules for electromagnetic transitions [8].

- For $\Delta T = 1$ transitions ($T_f = T_i \pm 1$), the (reduced) matrix elements of analogue transitions in mirror nuclei or between respective analogue states should be identical, since they are governed only by the isovector term.
- In transitions between the states of the same isospin ($T_i = T_f = T$), both isoscalar and isovector terms contribute, and the matrix element for analogue transitions within an isobaric multiplet exhibits a linear trend as a function of M_T:

$$\langle J_f M_f; T M_T | \hat{O}_{LM} | J_i M_i; T M_T \rangle = \langle J_f M_f | \hat{O}_{LM}^{(0)} | J_i M_i \rangle$$
$$+ \frac{M_T}{\sqrt{T(T+1)(2T+1)}} \langle J_f M_f; T || \hat{O}_{LM}^{(1)} || J_i M_i; T \rangle. \tag{11}$$

- Another specific rule can be established for electric dipole operator. In the lowest order of the long-wavelength approximation, the electric-dipole ($E1$) operator is an isovector operator:

$$\hat{O}(E1) = \sum_{k=1}^A e(k)\vec{r}(k) = \sum_{k=1}^A \left(\frac{1}{2} - \hat{t}_3(k)\right) e\vec{r}(k). \tag{12}$$

Hence, $E1$ transitions between the states of the same isospin ($T_i=T_f=T$) in $N = Z$ nuclei are forbidden by the isospin symmetry because of the vanishing Clebsch–Gordan coefficient, $(T\,0\,1\,0|\,T\,0\,) = 0$ (see Equation (11)).

Finally, isospin selection rules govern also nuclear reactions (see also, e.g., Refs. [9–11], for specific topics). Restricting ourselves to nuclear decays, only nucleon, two-nucleon and α-particle emission are mentioned here: for example, for isospin-allowed proton emission, the difference in isospin between the initial and final states is $\Delta T = 1/2$; for two-proton emission, it is $\Delta T = 1$; α emission should be consistent with $\Delta T = 0$.

Observation of isospin-forbidden decay modes indicates explicit isospin-symmetry breaking and the presence of isospin mixing in nuclear states.

1.2. Isospin-Symmetry Breaking

Although isospin symmetry proved to be quite a useful concept in nuclear and particle physics, which helps to simplify theoretical modeling of the nucleon–nucleon interaction and provides an efficient framework for the nuclear many-body problem, experimental evidence has been accumulated on the breaking of isospin symmetry.

First, it is known that isobaric multiplets are not degenerate. The differences in energy between states forming an isobaric multiplet are called *Coulomb displacement energies*, since the Coulomb interaction is the main contributor to the effect. Such splittings can be explained within *dynamical breaking* of isospin symmetry, as was pointed out in Section 1.1. However, observation of isospin-forbidden decays, i.e., decays which break isospin selection rules, indicates that isospin is not a good quantum number, and there is a certain amount of isospin mixing in nuclear states. To describe such phenomena, one must introduce an explicit breaking of isospin symmetry within a nuclear structure model. Development of microscopic approaches for an accurate description of isospin-symmetry breaking is important not only for understanding the structure and decay of proton-rich nuclei, but also for the evaluation of nuclear-structure corrections to weak processes in nuclei. Taking isospin-symmetry breaking into account may also help to improve our knowledge of certain reactions involving proton-rich nuclei, which are crucial for nuclear astrophysics.

At the nuclear level, isospin symmetry is broken mainly due to the Coulomb interaction among protons (a long-range component of the electromagnetic interaction between protons), and to a minor extent by the proton and neutron mass difference and the presence of the charge-dependent forces of nuclear origin (short-range). At the quark level, these causes can be rooted to the u and d quark mass difference and electromagnetic interactions between the quarks. The need for charge-dependent forces of nuclear origin was established long ago from the analysis of the nucleon–nucleon (NN) scattering data. For example, it is known that there are differences in the neutron–neutron (a_{nn}), proton–proton (a_{pp}, with electromagnetic effects being subtracted) and neutron–proton (a_{np}) $^1S_0$ (a $T = 1$ channel) scattering lengths [12,13]. Namely, the difference of a_{nn} and a_{pp},

$$a_{nn} - a_{pp} = 1.6 \pm 0.6 \text{ fm}, \tag{13}$$

is a signature of *charge-symmetry breaking* of the strong NN force; and the even larger difference between a_{np} and the average of a_{nn} and a_{pp},

$$\frac{1}{2}(a_{nn} + a_{pp}) - a_{np} = 5.64 \pm 0.40 \text{ fm}, \tag{14}$$

is known as the *charge-independence breaking* property.

Moreover, still long ago, Nolen and Schiffer [14] noticed that the Coulomb force alone cannot satisfactorily explain the binding energy differences in mirror nuclei if one requires the model to reproduce nuclear charge radii and vise versa (the so-called Nolen–Schiffer anomaly). The insufficiency of the two-body Coulomb interaction in reproduction of splittings of isobaric multiplets was also demonstrated in more refined shell-model

calculations (e.g., Refs. [15–17]). Many-body approaches must therefore, take into account short-range charge-dependent components of the nucleon–nucleon interaction.

Henley and Miller [18] proposed to divide two-nucleon forces into four classes according to their isospin characters, namely,

- class I (V_I) are charge-independent forces $\{1, \hat{\mathbf{t}}(1) \cdot \hat{\mathbf{t}}(2)\}$;
- class II (V_{II}) are forces which break the charge independence, but preserve the charge symmetry of the two-nucleon system, $\{\hat{t}_3(1)\hat{t}_3(2)\}$;
- class III (V_{III}) are charge-symmetry breaking forces, which vanish in the neutron-proton system, $\{\hat{t}_3(1)+\hat{t}_3(2)\}$;
- class IV (V_{IV}) are forces which do not conserve the isospin of the two-nucleon system: $\{\hat{\mathbf{t}}(1) \times \hat{\mathbf{t}}(2), \hat{t}_3(1) - \hat{t}_3(2)\}$.

If, as an example the two-body Coulomb interaction, acting between protons, is considered, one may notice that it comprises terms of classes I, II and III, as seen in Equation (5). It is important to note that although class II and class III forces commute with the two-nucleon isospin operator, such forces do violate the isospin symmetry in an A-nucleon system with $A > 2$.

Isospin-symmetry breaking two-nucleon forces have been constructed and explored in earlier meson-exchange models [12,19] and within the modern chiral effective field theory χEFT) [13,20–22]. The details of various contributions from hadronic mass splittings and electromagnetic processes can be found in the above-given references. From χEFT, the following hierarchy was deduced [20]: $V_I > V_{II} > V_{III} > V_{IV}$. In addition, charge-dependent three-nucleon (3N) forces have been constructed within χEFT see, e.g., the review [13] and references therein). Those may contribute to possible deviations of the IMME from its quadratic form, as discussed in Section 3.1 below.

Although charge-dependent realistic inter-nucleon interactions are frequently used in many-body calculations, in particular, in ab initio approaches, there have been few studies specifically focused on the degree of isospin-symmetry breaking. Nevertheless, ab initio Green's function Monte Carlo calculations with charge-dependent forces from the realistic Argonne v_{18} NN + Illinois-7 3N potential supplemented by more refined charge-dependent terms have been performed [23]. Quite good reproduction of the binding-energy differences in a few pairs of light mirror nuclei and the expected amount of isospin-mixing in ^{8}Be were reported. A significant feature of those calculations is that they introduced and demonstrated the role of class IV forces. Charge-dependent NN+3N forces from χEFT are used in state-of-the-art no-core shell model calculations for light nuclei [24,25], and the validity of isospin symmetry in electric quadrupole moments of mirror nuclei has been probed within the same theoretical approach in Ref. [26].

This review is devoted rather to the description of isospin-nonconserving phenomena in spectra and decays of heavier nuclei, for which a solution of the nuclear many-body problem needs an approach requiring effective charge-dependent interactions. Various theoretical frameworks aimed at a reliable description of isospin-symmetry breaking have been developed to deal with the problem. Among them are state-of-the-art shell-model calculations [15–17,27–35], including its no-core realization [36] and continuum-coupling extension [37], mean-field approaches and beyond (e.g., [38–47]) and others. Earlier comprehensive reviews on isospin symmetry and its breaking can be found in Refs. [9,48–50].

The present paper focuses rather on a particular theoretical approach to the problem, namely, on the nuclear shell model (e.g., see books [51–54]). Indeed, the shell model conserves all fundamental symmetries of atomic nuclei (such as angular momentum and particle number) and describes quite accurately individual states and transitions at low energies. This makes it an adequate approach for searching for tiny isospin-symmetry breaking effects. In the following sections, we highlight recent progress achieved by the isospin nonconserving shell model. A short summary of selected results has already been published in the proceedings of EuNPC2018 [55].

2. Formalism

The starting point of the shell model is a non-relativistic Hamiltonian for point-like nucleons containing nucleon kinetic energies and effective *NN* interactions (only two-body interactions are considered here):

$$\hat{H} = \sum_{k=1}^{A} \hat{T}_{\text{kin}}(k) + \sum_{k<l=1}^{A} \hat{V}_{\text{nucl}}(k,l)\,.$$ (15)

By adding and subtracting a one-body spherically symmetric potential (e.g., a harmonic-oscillator potential), one can rewrite the Hamiltonian as a sum of an independent-particle Hamiltonian ($\hat{H}_0$) and a residual interaction ($\hat{V}$):

$$\hat{H} = \sum_{k=1}^{A} \left[\hat{T}_{\text{kin}}(k) + \hat{U}(k) \right] + \left[\sum_{k<l=1}^{A} \hat{V}_{\text{nucl}}(k,l) - \sum_{k=1}^{A} \hat{U}(k) \right] = \hat{H}^{(0)} + \hat{V}\,.$$ (16)

The eigenstates of $\hat{H}$ ($\hat{H}\Psi_m = E_m\Psi_m$) are searched for in terms of a complete orthonormal set of eigenfunctions of $\hat{H}_0$ ($\hat{H}_0\Phi_m = E_{0m}\Phi_m$):

$$\Psi_m = \sum_{m'} C_{mm'}\Phi_{m'}\,.$$

Using this expansion, the eigenproblem is reduced for $\hat{H}$ to the diagonalization of the Hamiltonian matrix, $\langle\Phi_{m'}|\hat{H}|\Phi_m\rangle$, computed from single-particle energies of valence-space orbitals, $\varepsilon_{p,n}(a)$, and two-body matrix elements (TBMEs) of the residual interaction, $\langle ab; JMTM_T|\hat{V}|cd; JMT'M_T\rangle$ (a, b, c, d run over valence-space orbitals in a spherically symmetric mean field, i.e., $a = (n_a l_a j_a)$ and so on). As a result, one gets eigenvalues E_m and the corresponding sets of expansion coefficients $\{C_{mm'}\}$. If the nuclear Hamiltonian, which is rotational invariant, is also taken to be charge-independent (the proton and neutron single-particle energies are identical and TBMEs are independent from M_T with $T = T'$), its eigenstates are characterized by the angular momentum and isospin quantum numbers ($JMTM_T$), thereby forming degenerate spin (isospin) multiplets.

Since the model's space dimensions grow quickly as the number of particles increases, only for light nuclei can the shell model problem be solved for all nucleons considered in a model space comprised of many harmonic-oscillator shells. When using realistic internucleon interaction, the approach is referred to as an ab initio no-core shell model [24]. For heavier nuclei, the shell-model problem is formulated for valence nucleons only, occupying a model space consisting of one or two oscillator shells beyond a closed shell core. This restriction of the model space has been proved to be sufficient for low-energy nuclear structures. However, because of a severely truncated model space, one needs to derive a so-called *effective interaction*.

In this context, the isospin formalism helps to reduce the number of parameters. Nevertheless, construction of robust valence-space effective Hamiltonians remains a challenging and a long-standing problem of nuclear theory. Microscopic effective interactions have been constructed, for example, within the many-body perturbation theory, starting from the pioneering work in 60s [56,57] and continuing on into recent times (for reviews, see Refs. [58–60]). In spite of important advances, microscopic interactions are known to be less successful than more phenomenological parametrizations, based on the adjustment of TBMEs to selected data on nuclear spectra from a given model space. In particular, with two-nucleon forces only, the resulting effective interaction suffers from serious deficiencies in their monopole component [61]. This feature was ascribed to missing 3*N* forces. In addition, a number of theoretical issues in application of many-body perturbation theory to nuclear effective interaction problem have been raised regarding convergence of the expansion [62], which have not convincingly been answered yet.

In the last decade, new non-perturbative approaches to the construction of effective valence-space Hamiltonians have been put forward, based on unitary transformation

techniques—the in-medium similarity-renormalization group approach (IMSRG) [60,63] and the Okubo–Lee–Suzuki transformations of no-core shell-model solutions [64,65]. In addition, similar ideas have been implemented within the coupled-cluster method [66–68]. Moreover, some of these approaches, including modern many-body perturbation theory [69, 70], have successfully incorporated three-nucleon forces in their frameworks, producing state-of-the-art microscopic effective valence-space interactions from first principles.

In spite of all these developments, phenomenological effective interactions still remain a benchmark. Therefore, let us start the discussion of isospin-nonconserving (INC) Hamiltonians from a phenomenological perspective.

2.1. Phenomenological Approaches

Phenomenological effective Hamiltonians are typically isospin-conserving; therefore, the Coulomb contribution is usually evaluated and subtracted from the data before it is used in a fit. The resulting interactions are called realistic, and they can provide high accuracy in the description of nuclear excited states and transitions at low energies for a large set of nuclei (ideally, all nuclei) from a given model space. The most famous examples are the Cohen–Kurath Hamiltonians [71] in the p shell; the universal sd shell (USD) family of Hamiltonians [72,73], and Kuo-Brown modified KB3G [74] and GXPF1A [75] Hamiltonians in the pf shell.

An attractive option to construct an accurate INC Hamiltonian is thus to adopt a well-established charge-independent Hamiltonian as a lowest-order approximation and to add an INC term. The latter must contain the two-body Coulomb interaction and effective charge-dependent NN forces ($\hat{V}_{\mathrm{CD}}$), at least of classes II and III (no class IV forces are discussed here, but eventually, the framework can be extended to include them as well). Such an operator is a sum of an isoscalar, an isovector and an isotensor term:

$$\hat{V}_{\mathrm{INC}} = \hat{V}_{\mathrm{Coul}} + \hat{V}_{\mathrm{CD}} = \sum_{\lambda=0,1,2} \hat{V}_{\mathrm{INC}}^{(\lambda)}, \quad \text{where} \quad \begin{cases} \hat{V}_{\mathrm{INC}}^{(0)} = (v_{pp} + v_{nn} + v_{np}^{T=1})/3\,, \\ \hat{V}_{\mathrm{INC}}^{(1)} = v_{pp} - v_{nn}\,, \\ \hat{V}_{\mathrm{INC}}^{(2)} = (v_{pp} + v_{nn})/2 - v_{np}^{T=1}\,. \end{cases}$$

To describe the Coulomb effects of the core, an isovector one-body term is added which gives rise to the so-called *isovector single-particle energies*, $\tilde{\varepsilon}(a) = \varepsilon_p(a) - \varepsilon_n(a)$, where a runs over model-space orbitals. In lowest-order perturbation theory, the splitting of the isobaric multiplets is due to the expectation value of this operator; therefore, it is expressed by a quadratic polynomial in M_T, similarly to Equation (7):

$$\langle \Psi_{TM_T} | \hat{V}_{\mathrm{INC}} | \Psi_{TM_T} \rangle = E^{(0)}(\eta, T) + E^{(1)}(\eta, T)M_T + E^{(2)}(\eta, T)\left[3M_T^2 - T(T+1)\right].$$

In order to find the best set of parameters of $\hat{V}_{\mathrm{INC}}$ and isovector single-particle energies $\tilde{\varepsilon}_a$, one can perform a fit requiring that theoretical isovector and isotensor components allow one to reproduce experimentally deduced b and c IMME coefficients for a wide selection of lowest and excited isobaric multiplets with $T = 1/2, 1, 3/2, \ldots$. This procedure was first proposed in Ref. [15] and was used in the later work related to the sd-shell [16,27] and pf-shell and heavier nuclei [28]. Among various possible forms of $\hat{V}_{\mathrm{CD}}$, modelization of that term either by a ρ-exchange Yukawa-type potential (with a scaled meson mass) or by the $T = 1$ term of the isospin-conserving Hamiltonian in the isovector and isotensor channels resulted in similar quality fits [15,27]. At the same time, the use of the π-exchange potential was found to require much stronger renormalization of the two-body Coulomb force, and therefore, it was not retained.

Figure 1 shows the b coefficients for the lowest doublets and c coefficients for the lowest triplets obtained from such phenomenological interactions for sd-shell and pf-shell nuclei, in comparison with the experimental values. It is evident that the agreement between theory and experiment is remarkable. The root-mean-square (rms) deviations between theory and experiment represented in Figure 1 are 30 keV (95 keV) for b coefficients in the

sd (*pf*) shell and around 9 keV (25 keV) for the *c*-coefficients in the *sd* (*pf*) shell. One can observe that the description of the *pf*-shell *b* coefficients worsens towards the middle of the shell. By excluding data for $A = 59, 61, 63$, the rms deviation reduces to 55 keV. This problem seems to be linked to the difficulty in the description of nuclei from the upper part of the *pf* shell because of large dimensions involved, and may not be related to the form of the INC terms. Note also that more realistic forms of $\hat{V}_{CD}$ did not help to improve the fit [16].
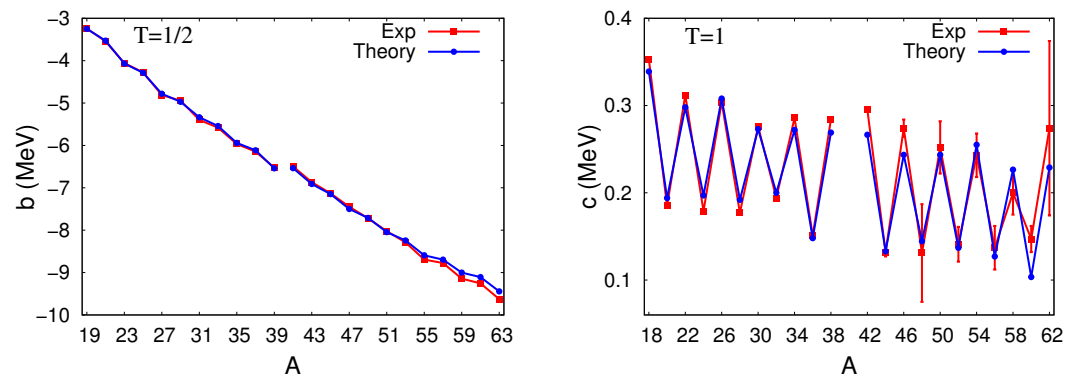
Figure 1. Experimental ("Exp") [5,76] and theoretical ("Theory") IMME *b* coefficients for the lowest doublets (**left**) and *c* coefficients for the lowest triplets (**right**) in the *sd* and *pf* shells. The *sd*-shell results were quoted from Ref. [27], and *pf*-shell calculations were performed with GX1Acd interaction [77]. See text for details.

As seen in Figure 1, the shell model well reproduces both the general trends and the fine structure of *b* and *c* coefficients. The latter considers the staggering *c* coefficients as a function of *A*, as well visible in Figure 1 (right): the *c* coefficients in $A = 4n + 2$ multiplets are systematically larger than those in $A = 4n$ (*n* being a positive integer). Similarly, the *b* coefficients in doublets and quartets form two families for $A = 4n + 1$ and $A = 4n + 3$, with opposite phases, however (for doublets, *b* coefficients are largest in $A = 4n + 1$ nuclei, and for quartets, they are largest for $A = 4n + 3$ nuclei). To amplify the effect, in Figure 2, the differences in *b* coefficients between *A* and $A - 2$ nuclei are plotted.
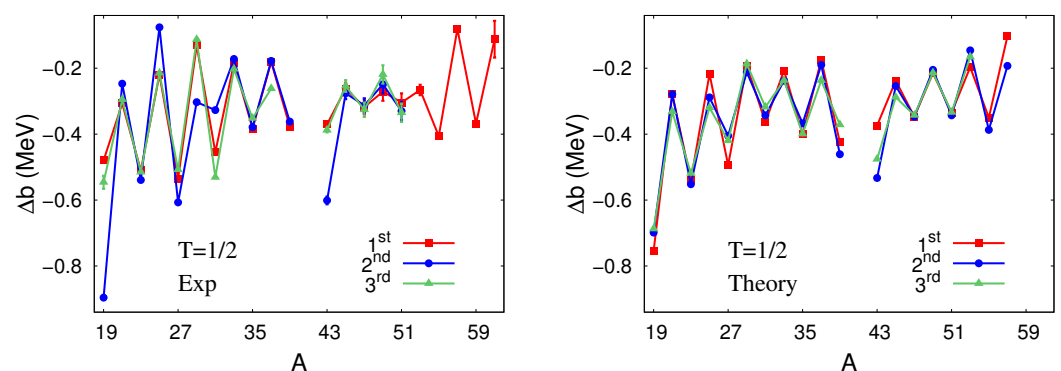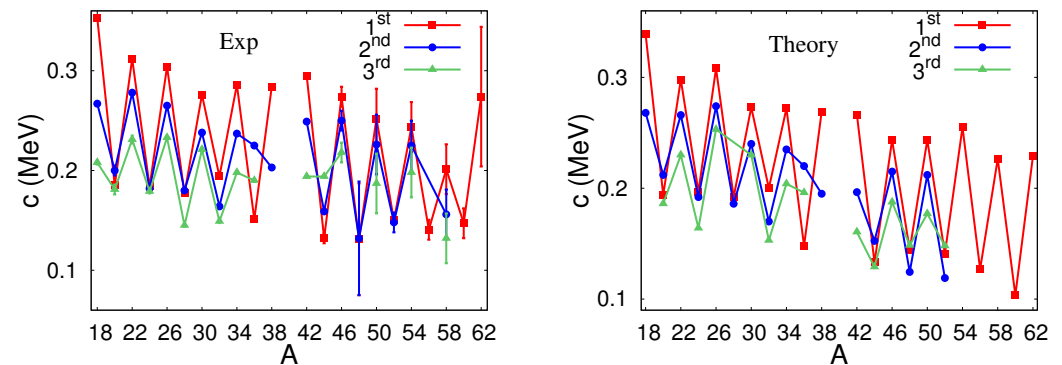

Figure 2. Experimental [5,76] (**left**) and theoretical (**right**) differences in IMME *b* coefficients (Δ_b) for the ground-state, first-excited and second-excited natural-parity $T = 1/2$ multiplets in the *sd* and *pf* shells. The *sd*-shell results were obtained with the interaction from Ref. [27], and *pf*-shell calculations were performed with GX1Acd interaction [77].

The staggering was noticed long ago and explained by the interplay between the Coulomb force and the pairing TBMEs [78]. It should be visibly present in *b* coefficients of multiplets with half-integer *T* and *c* coefficients of multiplets with integer values of *T*. The same conclusions have been reached [79] within a simpler macroscopic approach

supplemented by different proton and neutron average pairing gaps, which made it possible to grasp the main features of staggering.

Modern microscopic approaches [27,28,34,44,45] using realistic interactions well reproduce the effect. The main advantage of the shell-model type approaches is that they can describe b and c coefficients of excited states as well. Figures 2 and 3 show the differences among b coefficients, Δ_b and c coefficients for the three lowest positive-parity multiplets in doublets and triplets, respectively. Interestingly, that the amplitudes of oscillations diminish with excitation energy. This hints that the pairing effect gradually weakens as systems become more and more excited.

Figure 3. Experimental [5,76] (**left**) and theoretical (**right**) IMME c coefficients for the lowest, first-excited and second-excited $T = 1$ multiplets in the sd and pf shells. The sd-shell results were obtained with the interaction from Ref. [27], and pf-shell calculations were performed with GX1Acd interaction [77]. For $A = 42$, the data are given for $J^\pi = 0^+, 2^+, 4^+$ states. See text for details.

The approach described above can rather well reproduce an extended set of b and c coefficients and provides an attractive tool with which to predict binding energies and states in mirror systems using a method of Coulomb energy differences, described in Section 3.1 below. At the same time, a few drawbacks exist—namely, that it (i) does not allow one to predict nuclear masses on purely theoretical grounds, (ii) does not account for the so-called Thomas–Ehrman shift and (iii) it does not provide enough accuracy in the description of the differences in excitation energies of analogue states, usually referred to as Coulomb energy differences.

Another strategy was put forward by Zuker, Lenzi and collaborators in a series of papers starting from [17] (see also Refs. [80–82] for a recent review). The idea consists in modeling charge-dependent forces of nuclear origin with a few TBMEs, adjusted to reproduce the differences in excitation energies of isobaric multiplets relative to the lowest in energy multiplet. Those quantities are known as mirror energy differences (MEDs) and triplet energy differences (TEDs) in $T = 1$ multiplets, and they are related to the differences in b or c coefficients between the lowest multiplet and an excited one. For example, for triplets,

$$\text{MED}(J) = -2(b(J) - b_0),$$
$$\text{TED}(J) = 2(c(J) - c_0),$$

where b_0 (c_0) is a b (c) coefficient of the lowest triplet. Considered as a function of J along an excitation band (a pattern of excited states linked by pronounced electromagnetic transitions), MEDs and TEDs can bring pertinent information on nuclear structure effects. A vary accurate description has been achieved [17,80] of the pf shell by a phenomenological parameterization of various physical effects, such as changes in nuclear radius (or deformation) and electromagnetic corrections to the single-particle energies, with $\hat{V}_{\text{CD}}$ being modeled by a few $J = 0$ TBMEs in isovector and isotensor channels.

In Ref. [28], it was shown that modelization of V_{CD} by two $J = 0$, $T = 1$ TBMEs in the $f_{7/2}$ orbital and theoretically calculated single-particle energies was sufficient to reproduce the staggering behavior of b and c coefficients. This may not be surprising, since

we understand the staggering effect is due to the Coulomb contribution to the pairing-type matrix elements.

Later on, the approach was generalized to other model spaces using a more extended form of a charge-dependent term of nuclear origin as a number of TBMEs in Refs. [31,32]. MED and TED appear to be sensitive tools to unveil the structure of excited states, and in particular, TEDs and MEDs can shed light onto pair alignment process or on the shape evolution. Detailed study of the heavy $N = Z$ region allowed researchers to understand co-existing shapes and other effects in $A = 66, 70, 74, 78$ (e.g., [29,83]).

Moreover, MEDs have been shown [84] to depend linearly on the difference between neutron and proton radii, known as "neutron skin", and that they strongly correlate with the $s_{1/2}$-orbital occupation. In general, low-l orbitals, especially $s_{1/2}$ orbitals, are characterized by an extended radius and play thus a special role in nuclear structure. In particular, it was noted that MEDs of states having higher occupation of $s_{1/2}$ are unusually large. It turns out that states in proton-rich nuclei having high occupation of such an orbital experience a stronger shift with respect to their mirror states in neutron-rich partners. This is the essence of the so-called Thomas–Erhman effect [85,86]. Parameterizations of the charge-dependent forces mentioned above do not necessarily include this effect, which thus requires special care. In order to account for the Thomas–Ehrman shift, several approaches have been developed. For example, one can vary the energy of the proton $\varepsilon(s_{1/2})$ single-particle orbital (e.g., Ref. [87]) or quench TBMEs which involve $s_{1/2}$ orbitals [88]. Recently, a direct construction of TBMEs based on a simultaneous fit of isoscalar, isovector and isotensor terms has been undertaken, which lead to a few new types of USD interactions [34], aiming at consistent description of proton-rich and neutron-rich nuclei on similar grounds.

2.2. Semi-Phenomenological Approaches

A first step towards a more theoretical framework was to use a more realistic form of $\hat{V}_{\mathrm{CD}}$ on top of phenomenological wave functions. This was introduced in Ref. [16] for the sd shell but found to be less successful than a purely phenomenological charge-dependent term. More recently, in Ref. [33], microscopic charge-independence breaking pf-shell Hamiltonians have been constructed from the two-body CD-Bonn, Argonne v_{18} and chiral N^{3}LO (next-to-next-to-next-to-leading order) potentials on top of the phenomenological GXPF1A interaction. The authors compared theoretical IMME c coefficients as a function of the angular momentum in selected pf-shell nuclei with experimental data and conclude that the theory indicates too-strong of a contribution of the charge-independence breaking terms of nuclear origin.

2.3. Microscopic Approaches

A recent breakthrough in the construction of the NN interaction from effective field theories and advances in nuclear many-body methods led to the appearance of the first semi-microscopic and fully microscopic effective charge-dependent Hamiltonians. In particular, large-scale calculations for proton-rich nuclei in the extended $sdf_{7/2}p_{3/2}$ and $pfg_{9/2}$ model spaces with effective Hamiltonians, derived within many-body perturbation theory from χEFT NN+3N interactions, have been reported in Ref. [30].

Later on, valence space Hamiltonians were constructed within the IMSRG approach [35] based on two forces obtained within χEFT. The author tested the ability of their fully ab initio methods to reproduce the experimental IMME b and c coefficients for a large selection of nuclei of interest for superallowed β-decay applications with A between 10 and 74. Their conclusion is that although the major trend comes out correctly, their results are interaction-dependent and not precise enough to get the fine details.

Numerous modern theoretical investigations of nuclear properties are performed nowadays within ab initio approaches using charge-dependent realistic interactions (for example, those from χEFT). We believe that specific issues of isospin-symmetry breaking will definitely be addressed in forthcoming studies.

3. Structure and Decay of Neutron-Deficient Nuclei

Development of charge-dependent Hamiltonians has its ultimate goal of providing an accurate description of nuclei along the $N = Z$ line and proton-rich nuclei, making it possible to describe the signatures of isospin-symmetry breaking. This Section gives examples of how theoretical IMME coefficients can serve to predict nuclear masses and excited states in mirror nuclei, and it summarizes the progress in the description of isospin-forbidden transitions. The latter provide important tests of isospin mixing in nuclear wave functions to validate theoretical models.

3.1. IMME Coefficients for Masses and Excitation Spectra of Proton-Rich Nuclei

It was recognized long ago that the quadratic IMME, Equation (8), been successful throughout the nuclear chart, can provide a powerful method to determine masses, called the method of Coulomb displacement energies [28,79,89–92]. Namely, the mass excess of a proton-rich nucleus (with $M_T = -T$) on the basis of an experimental mass excess of its neutron-rich mirror (with $M_T = T$) and the theoretical b coefficient as

$$\mathcal{M}(\eta, T, M_T = -T) = \mathcal{M}(\eta, T, M_T = T) - 2\, b(\eta, T)\, T\,. \tag{17}$$

If theoretically Coulomb displacement energies are calculated, then they can be used straight instead of $2bT$ in Equation (18), as is done in Ref. [28,92]. Since the IMME is also applicable to describe excited multiplets, the method can be used to predict the positions of excited states in proton-rich nuclei.

Even more precise determination of the energy-level position is possible in triplets if two of three members of an isobaric multiplet are known experimentally:

$$\mathcal{M}(\eta, T, M_T = -1) = 2\mathcal{M}(\eta, T, M_T = 0) - \mathcal{M}(\eta, T, M_T = 1) + 2c(\eta, T)\,. \tag{18}$$

Since the rms (root-mean-square) deviation for c coefficients is typically smaller than that for b coefficients, one would expect to have a smaller theoretical uncertainty value. These methods can be advantageous for determination of the level in proton-rich nuclei of astrophysical interest (e.g., [93]), as pointed out in Section 5.

The methods described above rely on the quadratic IMME given by Equation (8). Indeed, for isobaric mutliplets with $T > 1$, which involve more than three members, deviations from the quadratic law can be expected. An extended IMME equation would include terms proportional to M_T^3 and M_T^4, i.e.,

$$\mathcal{M}(\eta, T, M_T) = a(\eta, T) + b(\eta, T)M_T + c(\eta, T)M_T^2 + d(\eta, T)M_T^3 + e(\eta, T)M_T^4\,, \tag{19}$$

which can be tested on quartets and quintets. Up till now, very few cases of non-zero d or e coefficients have been reported [5,6,94]; see also Refs. [95,96] and references therein. Typical values reach tens of keV.

Theoretically [94,97], deviations from a quadratic IMME are possible due to the presence of charge-dependent three-nucleon forces and/or due to isospin-mixing with nearby states. It is worth noting that the diagonalization of an INC shell-model Hamiltonian can generate an extended IMME, and several calculations have been reported [96,98]. To understand the challenge of getting reliable estimations of cubic and quartic terms on purely theoretical grounds, it is sufficient to notice that the rms errors of b and c coefficients are of the same order of magnitude or even larger than possible non-zero values of d and e coefficients. To avoid these ambiguities, a dedicated analysis constraining theory by available experimental information on $A = 32$ quintet have recently been performed [99]. Further efforts towards required precision will be crucial to advance our understanding of the origin of the IMME beyond its quadratic form.

3.2. Isospin-Forbidden Decays

Observation of transitions violating isospin selection rules, pointed to in the Introduction, signifies that the states are not pure in isospin. To predict theoretically the magnitudes of isospin impurities based on a fully microscopic calculation represents quite a complicated task. This can be understood as follows. In the shell model discussed here, isospin impurities arise from mixing of states of the same spin and parity but different isospin, if charge-dependent forces are present. Let us consider the simplest case of just two eigenstates of a charge-independent Hamiltonian, $|J^\pi, T\rangle$ and $|J^\pi, T'\rangle$, of isospin T and T', respectively. Inclusion of a charge-dependent interaction will result in new eigenstates, being linear combinations of unperturbed states, as

$$|a, J^\pi\rangle = \sqrt{1 - x^2}|J^\pi, T\rangle + x|J^\pi, T'\rangle$$
$$|b, J^\pi\rangle = \sqrt{1 - x^2}|J^\pi, T'\rangle - x|J^\pi, T\rangle \,.$$

The mixing amplitude, x, in the first order is given by the ratio of the isospin-mixing matrix element and the energy difference between the two states:

$$x \sim \langle J^\pi, T|V_{\mathrm{INC}}|J^\pi, T'\rangle / \Delta E \,.$$

It is known that it is difficult to predict theoretically the energy difference between states, especially for an odd–odd nucleus. Uncertainties of a few hundred keV may result in huge uncertainty on the mixing probability. However, we would like to require from theory to robustly predict the value of the mixing matrix element, $\langle V_{\mathrm{INC}}\rangle$. In practice, there could be many-state mixing, and the theory should able to deal with such a problem.

Mixing matrix elements depend strongly on the structure of the states considered, and therefore require in each case a dedicated calculation. Systematic calculations of $\langle V_{\mathrm{INC}}\rangle$, and distinction between its long-range (Coulomb) and short-range contributions, may bring interesting information, especially when compared to available experimental data (see Refs. [16,49] for an earlier study). From various specific calculations, it seems that typical values of $\langle V_{\mathrm{INC}}\rangle$ are between a few keV to a few tens of keV. Maximum values are 150 keV in *p*-shell nuclei [23,100], around 100 keV for *sd*-shell nuclei [16] and about 50 keV in the *pf* shell [101]. These estimations are in agreement with the largest observed values reported until now: $-145(20)$ keV for ^{8}Be in the *p* shell [100], 106(40) keV for ^{24}Mg [102] in the *sd* shell and 40(23) keV for ^{56}Cu [103] in the *pf* shell. Although theoretical uncertainty on energy differences between admixed states hampers direct predictions of isospin impurities from theory, it often turns out that combining calculations with experimental data may be sufficient to constrain predictions, as illustrated in Section 3.2.3 below.

3.2.1. Isospin-Forbidden β-Decay

To shed light on possible isospin impurities in nuclear states, one must appeal to isospin-forbidden transition probabilities. Let us remark that the only model-independent way to extract the amount of isospin-mixing from experiment is provided by Fermi β-decay [49]. Since the Fermi operator (9) is given by the isospin ladder operators $\hat{T}_\pm$, its matrix element between members of an isobaric multiplet can be expressed as

$$|M_{\mathrm{F}}^0| = |\langle T, M_T \pm 1|\hat{T}_\pm|T M_T\rangle| = \sqrt{(T + M_T)(T - M_T + 1)} \,. \tag{20}$$

In isospin-symmetry limit, the whole strength would feed the IAS. A measured depletion of the Fermi strength from the IAS or observation of Fermi transitions to non-analogue states can bring information on the amount of isospin mixing in the IAS. In addition, if a $M_T > 0$ nucleus β^+ (β^-) decays, then the mixing is dominantly present in the parent (daughter) nucleus, and inversely for a $M_T < 0$ nucleus. Then, the isospin-forbidden Fermi-matrix element in a non-analogue state can be estimated as $|M_{\mathrm{F}}^{IF}| = |x||M_{\mathrm{F}}^0|$.

Special cases of purely Fermi, non-analogue $0^+ \rightarrow 0^+$ transitions are known, and they bring important information for the tests of the weak interaction in nuclear decays [104].

Distribution of the non-analogue Fermi strength, as experimentally measured recently in ^{62}Ga [105], can shed light on the mixing matrix elements to cross-check the theory.

Transitions between states of the same (but non-zero) angular momentum, $J^\pi \to J^\pi$ ($J \neq 0$), are governed by both Fermi and Gamow–Teller components of the β-decay operator. A separation of the Gamow–Teller matrix element is an experimental challenge, bringing, however, direct knowledge on on isospin impurities, as elaborated in Refs. [49,106,107].

3.2.2. Signatures of Isospin-Symmetry Breaking from Electromagnetic Transitions

Observation of other isospin-forbidden decays requires theoretical calculations of corresponding nuclear processes for extraction of the mixing probability. For example, electromagnetic transitions which violate isospin selection rules propose another possibility to test the degree of isospin-symmetry breaking.

Electric dipole transitions play a special role in these explorations due to a specific isovector character of the operator; see Equation (12). In particular, in Section 1.1, it was mentioned that $E1$ transitions between the states of the same isospin in self-conjugate ($N = Z$) nuclei are forbidden by isospin symmetry. A few cases of observation of weak $E1$ transitions in $N = Z$ nuclei between states of the same isospin have been reported [108,109]. This indicates breaking of isospin symmetry in the states involved in the decay. The shell-model calculation of individual $E1$ transition rates is hampered by the fact that the model space should contain orbitals of different parities, which could also lead to a center-of-mass motion. Given that the center-of-mass separation is only approximate, it is a challenge to give a precise estimation of the $E1$ strength. Observed enhancements of $E1$ rates in $N = Z$ nuclei and enhanced asymmetries of mirror $E1$ transitions can be related to the giant isovector monopole resonance [109].

An original idea of using $E2/M1$ (electric quadrupole/magnetic-dipole) mixing ratio of decays in a self-conjugate nucleus ^{54}Co has been elaborated in Ref. [110] to pin down isospin impurities in a 4^+ doublet.

Electromagnetic transitions between isobaric analogue states provide other possibilities to test isospin selection rules. For example, linear dependence of the $E2$ matrix elements on M_T in $\Delta T = 1$ analogue transitions have been explored experimentally in a number of triplets (see Refs. [111,112] and references therein), and tests of equality of isovector matrix elements in mirror systems have been carried out [113,114].

An interesting idea to extract the amount of isospin mixing from $E1$ transition rates in mirror nuclei has been proposed and explored in Ref. [115].

Other possibilities to deduce isospin mixing in nuclear states from electromagnetic responses have been explored, e.g., in electron-scattering experiments [116] or via excitation of giant dipole resonance in $N = Z$ nuclei, e.g., in Refs. [117–119].

3.2.3. β-Delayed Proton, Diproton or α Emission

Nucleon(s) emission may serve as a stringent test of isospin purity [120]. Interesting cases are provided by β-delayed proton (or two-proton, α) emission when an IAS, populated in the β-decay, is located beyond the corresponding particle separation threshold [121,122]. As follows from a typical energy balance, in this case the proton (two-proton, alpha) emission from the IAS (J^π, T), populated in the β-decay of a $M_T < 0$ precursor, is forbidden by isospin symmetry (see Figure 4). Observation of such processes evidences the presence of isospin mixing, mainly, in the IAS which is surrounded by states of another isospin, (J^π, $T - 1$). A large amount of mixing can be deduced from the missing Fermi strength. However, small amounts may be hidden by experimental uncertainties.
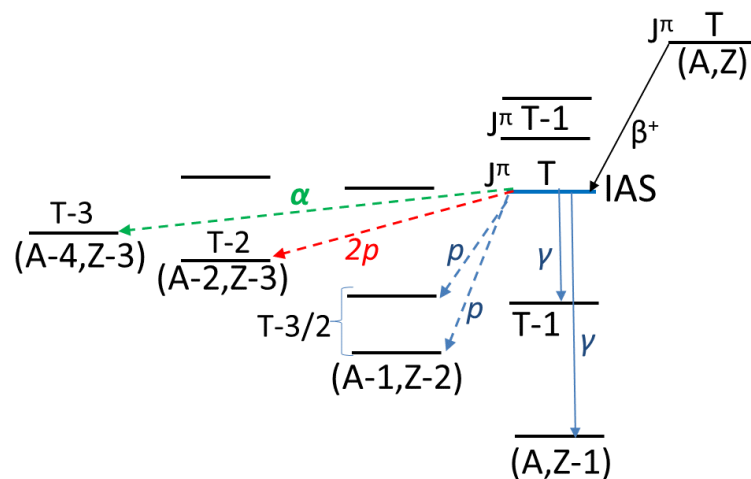
Figure 4. Schematic picture of β-delayed p, γ, $2p$ and α emission from an IAS. See text for details.

To deduce spectroscopic factors from isospin-forbidden proton emission on purely theoretical grounds is challenging [120,123]. Nevertheless, recently, it has been shown that one can deduce isospin mixing using experimental proton-γbranching ratios in the case of β-delayed $p\gamma$-emission [101,124] (two-proton or α emission were supposed to be absent or negligible in that study). Since the proton to γ-decay branching ratio for the IAS, $I_p^{\text{IAS}}/I_\gamma^{\text{IAS}}$, equals to the ratio of the corresponding widths, with the help of the theoretical electromagnetic width, $\Gamma_\gamma^{\text{IAS}}$, one can extract the proton width of the IAS as

$$\Gamma_p^{\text{IAS}} = \Gamma_\gamma^{\text{IAS}} \frac{I_p^{\text{IAS}}}{I_\gamma^{\text{IAS}}}. \tag{21}$$

Generally, the shell model provides a relatively robust description of electromagnetic widths, if experimental energies are used. Deduced proton widths are important in astrophysics applications. For example, radiative proton capture is an inverse process, where a nucleus capturing a proton gets excited to a specific level and is de-excited by γ emission. Proton and electromagnetic widths are thus essential ingredients with which to estimate the contribution of resonant capture.

In addition, if the angular momentum, l, of the proton is unambiguously determined (as in the decay from 0^+ state), from Equation (21) one can deduce the spectroscopic factor for an isospin-forbidden proton emission from the IAS. To this end, one can estimate theoretical single-particle proton width, Γ_{sp}^{IAS}, of the IAS and express the spectroscopic factor as

$$S_p^{\text{IAS}} = \frac{\Gamma_\gamma^{\text{IAS}}}{\Gamma_{sp}^{\text{IAS}}} \frac{I_p^{\text{IAS}}}{I_\gamma^{\text{IAS}}}. \tag{22}$$

Let us remark that this estimation does not rely on the isospin mixing in the IAS, which would depend on energies of admixed states, but only on the experimental ratio of proton and gamma intensities and on the calculated width.

If a two-state mixing hypothesis approximately holds, for example, when the IAS is mostly mixed with a single nearby non-analogue state (J^π, $T-1$), then one can approximately estimate the amount of isospin mixing in the IAS. Namely, using the shell-model value for the spectroscopic factor of the admixed state, $S_p^{\text{T}-1}$, the probability of mixing can be expressed as $x^2 = S_p^{\text{IAS}}/S_p^{\text{T}-1}$. This procedure can be generalized to include isospin-forbidden $2p$ or α-particle emission from the IAS.

For several measured proton branches that form the IAS, one can apply the above formalism to each of them separately, since relation (21) holds:

$$\Gamma_{p,i}^{\text{IAS}} = \Gamma_\gamma^{\text{IAS}} \frac{I_{p,i}^{\text{IAS}}}{I_\gamma^{\text{IAS}}} . \tag{23}$$

Proceed to extract spectroscopic factors and isospin mixing, if a two-level mixing model is applicable. This proposes an interesting possibility to cross-check the values of x^2 deduced from various branches. Such cases of β-delayed $p\gamma$ emission from an odd A precursor have also been reported (see, e.g., Refs. [121,122,125]).

Actually, one can also determine an approximate value of isospin mixing in the IAS in a two-level mixing case, even if the set of quantum numbers (nlj) characterizing the emitted proton is not unique. In this case, the proton width is a sum of contributing partial widths corresponding to all allowed orbitals from a given model space, e.g., $\Gamma_p^{\text{IAS}} = \sum_{nlj} S_p^{\text{IAS}}(nlj) \Gamma_{sp}^{\text{IAS}}(nlj)$. Therefore, providing shell-model values of isospin-allowed spectroscopic factors, $S_p^{T-1}(nlj)$, one can estimate the amount of isospin impurity of the IAS to be

$$x^2 = \frac{\Gamma_p^{\text{IAS}}}{\sum_{nlj} S_p^{T-1}(nlj) \Gamma_{sp}^{\text{IAS}}(nlj)} , \tag{24}$$

where Γ_p^{IAS} is deduced as in Equation (21) and the denominator is evaluated theoretically. Finally, individual spectroscopic factors (for each nlj channel) for isospin-forbidden proton emission can be obtained as $S_p^{\text{IAS}}(nlj) = x^2 S_p^{T-1}(nlj)$ The uncertainty of theoretical estimation increases in this case, since a few theoretical quantities have to be used. In general, one should also remember that small spectroscopic factors (below 0.1) carry a significant theoretical uncertainty and this may prohibit extraction of the detailed information according to the proposed method.

4. Theoretical Isospin-Symmetry Breaking Corrections to Weak Processes in Nuclei

At present, many-body calculations for nuclear structure are required to link experimental information on weak processes involving nuclei to the underlying theories of fundamental interactions. In this context, the nuclear shell model is among the most favorite tools to provide nuclear matrix elements necessary for the tests of the symmetries of the standard model and for the searches for physics beyond it. Those can be probed in nuclear β-decay, but also in charge–exchange reactions or, eventually, in muon capture experiments. Calculations allowing to account for isospin-symmetry breaking may become vital in studies of individual transitions involving proton-rich nuclei and nuclei along $N = Z$ line.

The discussion below focuses on two activities related to the study of beta decay, which can be described by an effective axial-vecor and vector, $V-A$, interaction Hamiltonian,

$$\hat{H}_{V-A} = \frac{G_V}{\sqrt{2}} \hat{J}_\mu^\dagger \hat{j}^\mu + \text{h.c.}, \tag{25}$$

where $\hat{J}_\mu^\dagger$ ($\langle j^\mu \rangle$) is hadronic (leptonic) weak current, the index μ represents the space-time 4-vector index and takes value 0 (time),1, 2, and 3 (space), "h.c." stays for "hermitian conjugate", and G_V is the weak-interaction coupling constant responsible for this semi-

leptonic decay. The most general form of a Lorentz-covariant form of the vector and axial-vector nucleon currents read

$$\hat{J}_\mu^\dagger = \hat{V}_\mu + \hat{A}_\mu \tag{26}$$

$$\hat{V}_\mu = i\overline{\psi}_p \left(g_V(k^2)\gamma_\mu + \frac{g_W(k^2)}{2m_N}\sigma_{\mu\nu}k_\nu + ig_S(k^2)k_\mu \right)\psi_n \tag{27}$$

$$\hat{A}_\mu = i\overline{\psi}_p \left(g_A(k^2)\gamma_\mu + \frac{g_T(k^2)}{2m_N}\sigma_{\mu\nu}k_\nu + ig_P(k^2)k_\mu \right)\gamma_5\psi_n \tag{28}$$

where ψ_p and ψ_n are nucleon field operators, m_N is the nucleon mass; k_μ is the 4-momentum transferred from hadrons to leptons; $\sigma_{\mu\nu} = [\gamma_\mu, \gamma_\nu]/2i$ and γ_μ are Dirac matrices. The six form-factors are arbitrary real functions of Lorentz invariants of k^2, to be compatible with time-reversal invariance. At low momentum transfer, they are known as the vector (g_V), weak magnetism (g_W), scalar (g_S), axial-vector (g_A), tensor (g_T) and pseudo-scalar (g_P) coupling constants.

The six terms have definite properties under the $\hat{G}$-parity transformation, which is a combination of charge-conjugation ($\hat{C}$) and rotation in isospin space over 180 degrees about the 2-axis ($\hat{G} = \hat{C}\exp(i\pi\hat{T}_2)$). Those which transform as leading-order vector and axial-vector terms are called first-class currents, and those which have opposite transformation properties are called second-class currents. Of the latter type are the induced scalar term in the vector current and induced tensor term in the axial-vector current.

Various constraints on these coupling constants come from the symmetries underlying the standard model [126]. The most stringent condition is provided by the conserved vector current (CVC) hypothesis, which is based on the similarity in structure of the vector weak current and the isovector electromagnetic current. From CVC, it follows that the vector and weak-magnetism form factors are related to their electromagnetic counterparts, in particular, $g_V(k^2 \to 0) = 1$. This symmetry also implies that the induced scalar term vanishes ($g_S = 0$).

For the axial-vector current, only a partially conserved axial-vector current hypothesis exists, and it is less restrictive: it allows one to relate the main axial-vector coupling constant to the pion–nucleon coupling constant by famous Goldhaber–Trieman relations.

Nuclear β-decay experiments provide an excellent ground to test the structure of these currents and experimentally determine the magnitude of the coupling constants (see extensive reviews [127,128]). Two particular domains are described below, when theoretical calculation of nuclear matrix elements is required, along with an accurate treatment of isospin-symmetry breaking.

4.1. Superallowed Fermi β-Decay

The most prominent application of the theoretical formalism exposed just above is the calculation of realistic Fermi-matrix elements for β-decay between 0^+ states or between the mirror states in $T = 1/2$ nuclei [129].

Indeed, Fermi type β-decay is governed uniquely by the vector part of the weak current. According to the CVC hypothesis, the absolute *Ft* values of such transitions in various emitters with a given isospin T should be the same. If this feature holds, from *Ft* one can deduce the vector's coupling constant, G_V, that is responsible for this semi-leptonic decay ($u \to de^+\nu_e$). Combining G_V with the value of fundamental weak coupling constant G_F obtained from a purely leptonic muon decay ($\mu^+ \to e^+\nu_e\overline{\nu}_\mu$), one can determine the absolute value of the $|V_{ud}| = G_V/G_F$ matrix element of the Cabibbo–Kobayasi–Maskawa (CKM) quark-mixing matrix:

$$V_{\text{CKM}} = \begin{pmatrix} V_{ud} & V_{us} & V_{ub} \\ V_{cd} & V_{cs} & V_{cb} \\ V_{td} & V_{ts} & V_{tb} \end{pmatrix}.$$

Numerical values of CKM matrix elements are important for the unitarity tests, such as the normalization condition for its first row: $|V_{ud}|^2 + |V_{us}|^2 + |V_{ub}|^2 = 1$.

The absolute Ft value is obtained from the experimentally deduced ft value after incorporation of a few non-negligible theoretical corrections [130] as defined by the following equation:

$$Ft^{0^+ \to 0^+} \equiv ft^{0^+ \to 0^+}(1 + \delta'_R)(1 + \delta_{NS} - \delta_C) = \frac{K}{|M_F^0|^2 G_V^2(1 + \Delta_R)}. \qquad (29)$$

Here, f is the statistical rate function calculated from the decay energy, t is the partial half-life of the transitions, $K = 2\pi^3\hbar \ln 2(\hbar c)^6/(m_e c^2)^5$, $|M_F^0|$ is the Fermi-matrix element in the isospin-symmetry limit (20), $\hbar$ is the reduced Planck's constant, c is the speed of light, and Δ_R, δ'_R and δ_{NS} are transition-independent, transition-dependent and nuclear-structure-dependent radiative corrections; and δ_C is the isospin-symmetry breaking correction due to the lost analogue symmetry between the parent and the daughter nuclear states. The detailed description of the electroweak corrections and the current status in the field can be found in the latest survey by Hardy and Towner [130]. The most prominent feature discussed in recent years is an updated value of the transition independent term, Δ_R, which was re-evaluated using the formalism of the effective field theory, and this brought fragility to the unitarity tests [131].

The present discussion focuses on the isospin-symmetry breaking correction, δ_C. This correction is defined as a deviation of the squared realistic Fermi-matrix element from its isospin-symmetry value: $|M_F|^2 = |M_F^0|^2(1 - \delta_C)$. Therefore, the estimation of δ_C requires an accurate calculation within a nuclear-structure model which can account for the broken isospin symmetry.

There have been lots of efforts within various theoretical approaches during a few decades already. Figure 5 summarizes predictions from different calculations for the 13 best known transitions (by now, the decay of ^{26}Si has been added to this dataset).
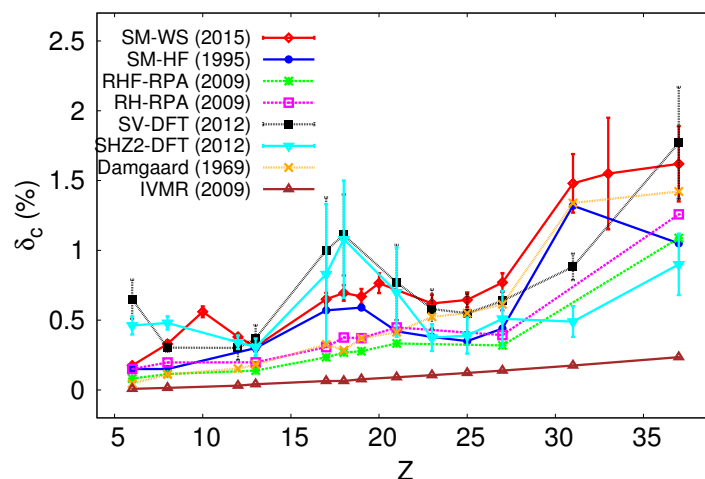
Figure 5. Isospin-symmetry breaking correction, δ_C, from various theoretical approaches: SM-WS(2015) [130], SM-HF(1995) [132], RHF-RPA(2009) [39], RH-RPA(2009) [39], SV-DFT(2012) [42], SHZ2-DFT(2012) [42], Damgaard(1969) [133], IVMR(2009) [134]. Figure is adapted from Ref. [135].

The values obviously diverge. In addition, to note is that theoretical approaches assign important uncertainties to their values (those which present associated uncertainties). Currently, evaluation of δ_C provides the largest contribution to the Ft-value uncertainty.

As has been demonstrated in Section 2 above, the INC shell model represents a well-suited tool for the δ_C calculation. By expressing the Fermi-matrix elements in the second quantization, one gets:

$$M_{\rm F} = \langle \Psi_f | \hat{T}_+ | \Psi_i \rangle = \sum_\alpha \langle f | \hat{c}^\dagger_{\alpha_n} \hat{c}_{\alpha_p} | i \rangle \langle \alpha_n | \hat{t}_+ | \alpha_p \rangle \,, \tag{30}$$

where $\hat{c}^\dagger_\alpha$ and $\hat{c}_\alpha$ are nucleon creation (destruction) operators; α denotes a full set of spherical quantum numbers, $\alpha = (n_a, l_a, j_a, m_a) \equiv (a, m_a)$ and the two ingredients of Equation (30) are (i) one body-transition densities:

$$\langle f | \hat{c}^\dagger_{\alpha_n} \hat{c}_{\alpha_p} | i \rangle \equiv \rho_\alpha \,, \tag{31}$$

and isospin single particle matrix elements, given by overlap integrals:

$$\langle \alpha_n | \hat{t}_+ | \alpha_p \rangle = \int_0^\infty R_{\alpha_n}(r) R_{\alpha_p}(r) r^2 dr \equiv \Omega_\alpha. \tag{32}$$

Here, R_α denotes the radial part of the single-particle wave function.

It has been pointed out by Miller and Schwenk [136,137] that the use of the exact isospin operator in Equation (30) would involve terms where the radial quantum number, n_α, for of a proton state, α_p, is different from that of a neutron state α_n. Up till now, all shell-model work [132,135,138,139] has been done within an approximation that allows one to express the radial overlaps by Equation (32).

Calculation of realistic Fermi-matrix elements implies the use of one-body transition densities computed using many-body states obtained from the diagonalization of an INC Hamiltonian, and the use of radial wave functions, obtained from a realistic spherical single-particle potential, such as Wood–Saxon (WS) or Hartree–Fock (HF) potential, instead of the harmonic oscillator. Therefore,

$$M_{\rm F} = \sum_\alpha \rho_\alpha \Omega_\alpha \,,$$

and the model-independent value (20) can be obtained from one-body transitions densities in the isospin limit (ρ^0_α) and harmonic-oscillator radial overlaps $(\Omega^0_\alpha = 1)$:

$$M^0_{\rm F} = \sum_\alpha \rho^0_\alpha \Omega^0_\alpha = \sum_\alpha \rho^0_\alpha$$

(the superscript "0" indicates that those quantities were calculated in the isospin limit). Therefore, there are two sources of isospin-symmetry breaking in the Fermi-matrix element: first comes from the difference in configuration mixing of the parent and daughter nuclei as obtained from the shell-model diagonalization of an INC Hamiltonian. The other is due to the deviation of the radial overlaps from unity, when calculated with realistic single-particle wave functions instead of the harmonic-oscillator ones. These deviations of one-body transitions densities and radial overlaps from their isospin-symmetry values are typically small. Keeping only linear terms in small quantities, one can express $|M_{\rm F}|^2$ as

$$|M_{\rm F}|^2 \approx |M^0_{\rm F}|^2 \Big[1 - \underbrace{\frac{2}{M^0_{\rm F}} \sum_\alpha \big(\rho^0_\alpha - \rho_\alpha \big)}_{\delta_{C1}} - \underbrace{\frac{2}{M^0_{\rm F}} \sum_\alpha \rho^0_\alpha (1 - \Omega_\alpha)}_{\delta_{C2}} \Big],$$

From this expression, it is seen that the correction splits into two terms according to the two sources of isospin-symmetry breaking mentioned above:

$$\delta_C \approx \delta_{C1} + \delta_{C2} \,.$$

To get δ_{C1}, it is sufficient to perform calculations with INC interactions. As has been discussed in Section 3, the theoretical value for a depletion of the Fermi strength in the IAS is due to the mixing of the IAS with non-analogue states (see Figure 6 (left)). Therefore, the position of those states is vital.
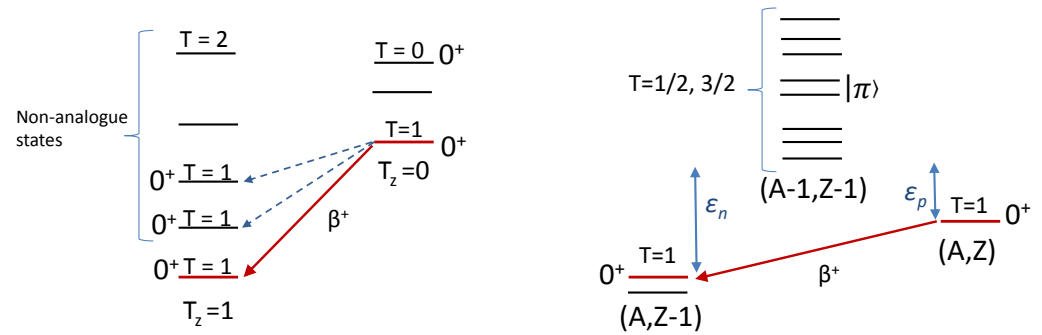
Figure 6. Schematic picture of the Fermi strength distribution in the daughter nucleus due to the isospin-symmetry breaking effects, as can be viewed from the shell-model's perspective. **Left**: depletion of the Fermi strength from an IAS because of non-analogue transitions. **Right**: insertion of the intermediate states to better constrain the radial part of the single-particle wave functions.

To avoid this uncertainty, one may scale the strengths of individual transitions to non-analogue states with the energy difference between those states and the IAS [138]:

$$\delta_{C1} = \delta_{C1}^{\text{th}} \left(\frac{\Delta E_{\text{th}}}{\Delta E_{\text{exp}}} \right)^2 .$$

Existing shell-model studies use various parametrizations of the INC Hamiltonian, ranging from realistic phenomenological fits [132,135,140] to individual parametrization of charge-dependent terms to each isobaric multiplet presented in Ref. [138,139]. Since this part of the correction is small, the results of both approaches are within typical uncertainties.

In addition to the isospin-symmetry breaking inside the model space, one has to replace harmonic-oscillator radial wave functions with realistic spherically symmetric wave functions from a WS or a HF potential, including Coulomb. This is the largest part of the correction; see Ref. [138] and references therein. A parametrization of a single-particle potential is crucial for the value of the correction. Due to this reason, potential parameters are adjusted to reproduce proton and neutron separation energies and nuclear charge radii. To achieve this goal, a calculation has to be done beyond the closure approximation. This means instead of inserts, a complete sum of intermediate nucleus states ($\{\pi\}$) in the Fermi-matrix element. Then, the radial-overlap correction can be expressed as

$$\delta_{C2} = \frac{2}{M_{\text{F}}^0} \sum_{\alpha,\pi} \langle f | \hat{c}_{\alpha_n}^\dagger | \pi \rangle^0 \langle \pi | \hat{c}_{\alpha_p} | i \rangle^0 (1 - \Omega_\alpha^\pi) .$$

The two ingredients are the spectroscopic amplitudes, $\langle f | \hat{c}_{\alpha_n}^\dagger | \pi \rangle^0$, obtained within the isospin-symmetry limit, and the radial-overlap integrals

$$\Omega_\alpha^\pi = \int_0^\infty R_{\alpha_n}^\pi(r) R_{\alpha_p}^\pi(r) r^2 dr ,$$

which now contain dependence on the excitation energy of the intermediate states π; see Figure 6 (right).

This opportunity to constrain theoretical calculations by experimental observables greatly helps to reduce uncertainty in the potential parameters and guaranties consistency of the results, as has been discussed in detail in Ref. [135]. In particular, the largest

contribution to theoretical uncertainty on δ_{C2} is because of the experimental uncertainty on the nuclear charge radii.

Up till now, systematic calculations with the WS potential are the only ones who produce corrections consistent with the CVC hypothesis within a non-zero confidence limit [141]. The use of the HF wave functions, pioneered by Ormand and Brown [132,140,142], has been explored by a few other groups as well [138,143,144]. Self-consistent HF potentials are not immediately appropriate for calculations and have to also be adjusted to give rise to experimental proton and neutron separation energies. The procedures exploited by various authors are somewhat different, and, in general, led to smaller corrections than those obtained from a WS potential. This issue has recently been explored in detail in Ref. [144]. In particular, the authors examined the role of previously neglected effects, taking care of the approximate elimination of spurious isospin-mixing, two-body center-of-mass corrections, exact treatment of the exchange Coulomb term and many others. Moreover, INC terms have been added to the energy-density functional. Those corrective terms indeed explain some of the difference between the HF and WS results, allowing to suppose that the remaining part of the difference is due to the need for correlations beyond the HF approximation. Further efforts towards more sophisticated theories should be addressed in future studies.

In spite of these challenges in the computation of theoretical corrections, nuclear $0^+ \to 0^+$ β-decay provides the best opportunity to test the CVC and to extract the V_{ud} value, among other ways (mirror transitions, neutron or pion beta decay) [130]. Therefore, it is reasonable to persist with efforts in improving theoretical modelization of the isospin-symmetry breaking correction.

4.2. β-Decay between Mirror T = 1/2 States

It was pointed also that β-decay between mirror states with $T = 1/2$, which are governed by both Fermi and Gamow–Teller operators, can also serve for the tests of the CVC hypothesis and extraction of V_{ud}, once the GT component is eliminated [130,145]. To this end, an additional correlation coefficient has to be measured. Similarly to $0^+ \to 0^+$ decay, the experimentally determined ft value has to be corrected for radiative effects and for isospin-symmetry breaking in decaying states. The shell-model framework relies on a similar expression of the realistic Fermi-matrix element, as discussed, with an intermediate state summation which involves a larger number of different states because of non-zero values of angular momenta involved. Currently achieved results are summarized in Ref. [129].

4.3. Gamow–Teller Transitions in Mirror Nuclei

Another long-standing application is related to the asymmetry of Gamow–Teller β-decay rates in mirror nuclei, defined as

$$\delta = \left| \frac{M_{GT}^+}{M_{GT}^-} \right|^2 - 1 \,, \tag{33}$$

where $M_{GT}^{\pm}$ are reduced matrix elements for mirror GT $\beta^{\pm}$ transitions. The initial interest in the topic was due to the fact that the contribution to that asymmetry may be due to the presence of the induced tensor term (g_T) in the axial-vector current; see Equation (28).

To pin down a possible manifestation of the induced tensor term, an accurate calculation of GT matrix elements, including isospin-symmetry breaking, is required. In the second-quantization formalism, the reduced matrix elements of the GT operator can be expressed as follows:

$$M_{GT}^{\pm} = \langle \Psi_f || \hat{O}_{GT}(\beta^{\pm}) || \Psi_i \rangle = \frac{1}{\sqrt{3}} \sum_{a,b} \langle J_f || [\hat{c}_a^\dagger \, \hat{c}_b]^{(1)} || J_i \rangle \langle a, m_{t_a} || \hat{\sigma} \hat{t}_+ || b, m_{t_b} \rangle \,, \tag{34}$$

where double bars denote reduction in angular momentum, and $\hat{\hat{c}}_{a,m_a} = (-1)^{j_a+m_a} \hat{c}_{a,-m_a}$. Again, realistic calculations should be ensured beyond the closure approximation, thereby inserting a complete sum over intermediate nucleus states. Several theoretical investigations have been performed from the 60s up to the present, without any indication on a possible application of the analysis to the weak-interaction problem because of high theoretical uncertainty of the nuclear wave functions (see Ref. [146,147] and references therein). Although experimental measurements of mirror transitions main an active field, the main impact of the results is on the structural aspects of the states involved in the decay. In this context, alternative constraints on the induced tensor current from β-α and β-γ angular correlation experiments tend to be much more advantageous [148,149].

5. Astrophysical Applications

One of the greatest motivations to explore the properties of nuclei is their need for nuclear astrophysics. Nuclear masses, half-lives, level densities, and nuclear, electromagnetic and weak-interaction reaction rates represent crucial ingredients for simulations and understanding of astrophysical processes [150]. In particular, the structure of neutron-deficient nuclei is important for comprehension of nucleosynthesis during stellar explosive hydrogen burning. Among the possible sites are X-ray bursts and novae outbursts.

Novae are understood as a result of thermonuclear runaway at the surface of a white dwarf within a binary star system. At high temperatures ($\sim 10^8$ K) and densities in O-Ne type novae, the break-out of the hot CNO (carbon-nitrogen-oxygen) cycle leads to nucleosynthesis of heavier elements $A \geq 20$ by mainly (p, γ), in competition with (α, p) and inverse reactions, with the end point around Ca [151]. In X-ray bursts [152,153], based on a neutron star accreting hydrogen matter within a binary system, the temperatures are even higher (up to 2×10^9 K), and radiative proton capture reactions involve proton-rich nuclei towards the proton-drip line, being the most important reaction type in nucleosynthesis with up to roughly $A \sim 100$ (rp process). Simulations of X-ray bursts exploit a huge set of nuclear reactions which have to be constrained.

For stable nuclei, the proton-capture reaction Q-values are relatively high, and the reaction rate may be approximated by a statistical model. For unstable (proton-rich) nuclei, Q values become small (in the order of a few MeV or less), and hence, the reaction rate is dominated by a few isolated resonances above the proton-emission threshold, together with a non-resonant reaction contribution in the energy range within a Gamow peak. In this case, accurate knowledge of resonance energies and decay widths is required.

Current state-of-the-art simulations are based on experimentally deduced information when it is available. If no data exist yet, then one can either deduce the missing information from mirror systems, assuming the isospin symmetry, or appeal to theory. Therefore, higher-precision theoretical calculations are important to reduce uncertainties.

Shell modeling is one of the approaches which can provide detailed information on nuclear states and transitions at low energies. The resonant part of a thermonuclear (p, γ) reaction rate for a single resonance can be expressed [154] as

$$N_A \langle \sigma vs. \rangle_r = 1.540 \times 10^{11} \, (\mu T_9)^{-3/2} \, \omega \, \gamma \, \exp\left(\frac{-11.605 \, E_r}{T_9}\right) \text{cm}^3 \, \text{s}^{-1} \, \text{mol}^{-1} \, , \quad (35)$$

where $\mu = A_p A / (A_p + A)$ is the reduced atomic mass number and E_r is the resonance energy above the proton-emission threshold (in MeV), T_9 is the temperature in GK. The resonance strength $\omega \, \gamma$ (in MeV) depends on the spins of initial J_i and final (resonance) J_f states, the partial proton width Γ_p for the entrance channel and gamma widths Γ_γ for the exit channel:

$$\omega\gamma = \frac{2J_f + 1}{2(2J_i + 1)} \frac{\Gamma_p \Gamma_\gamma}{\Gamma_{tot}} \, , \quad (36)$$

with $\Gamma_{tot} = \Gamma_p + \Gamma_\gamma$. The proton decay width depends on the resonance energy via the proton width, which could be estimated from a single-particle potential model and the

shell model's spectroscopic factor. In case of a few resonances, the resonant reaction rate represents a sum of single-resonance rates (35) over contributing final states.

The non-resonant part of (p, γ), the reaction rate is given by direct capture transitions to the ground or low-level states of the final nucleus.

A number of radiative proton-capture reaction rates have been evaluated with a good precision for sd-shell and pf-shell nuclei [155,156], since the shell model provides missing information on resonance states, proton and electromagnetic widths. The INC formalism is of particular interest for such problems. First, using theoretical IMME b coefficients, one can not only provide nuclear masses of proton-rich nuclei [28,91,92], but also determine positions of unknown resonances in a proton-rich nucleus, if the level scheme of a neutron-rich mirror nucleus is known experimentally. The necessity to account for isospin-symmetry breaking to get more accurate results was demonstrated first in Ref. [155] and followed in numerous studies. A use of theoretical c coefficients may even be more advantageous for an $M_T = -1$ nuclei if experimental information on $M_T = 0, 1$ exists (see, e.g., [93,157,158].) The cross-shell p-sd-pf model space is necessary for the description of negative parity resonances in sd-shell nuclei (see, e.g., Refs. [159,160]).

A particularly interesting result was obtained a few years ago, indicating that the Thomas–Ehrman effect may significantly change values of theoretical spectroscopic factors [87]. More attention therefore has to be paid to small values of spectroscopic factors. This also indicates that results on spectroscopic factors from mirror systems should be accepted with caution.

6. Conclusions and Perspectives

The nuclear shell model provides a powerful formalism with which to deal with tiny breaking of isospin symmetry in nuclear states. Currently, the most accurate results are due to phenomenological treatment of nuclear wave functions and parametrization of the INC terms of the Hamiltonian. Although more work is required to have a better handle on large model spaces, extended applications to structure and decay proton-rich nuclei and nuclei along the $N = Z$ line support experimental investigations. Important applications of that formalism exist, such as the calculation of isospin-symmetry breaking corrections for Fermi-matrix elements required to test the symmetries underlying the standard model. Finally, isospin-symmetry breaking is nowadays taken into account in the evaluation of thermonuclear reaction rates in proton-rich nuclei, which plays an important role in astrophysical simulations.

While phenomenological approaches still have to be pursued to assure solid support to experimental investigations, the eventual goal of nuclear theorists is to develop fundamental ab initio frameworks for many-body calculations towards a higher precision level that will be relevant for the isospin-symmetry breaking domain.

Abbreviations

The following abbreviations are used in this manuscript

CD	charge-dependent
CKM	Cabbibo-Kobayashi-Moskawa
CNO	carbon-nitrogen-oxygen
CVC	conserved vector current
$E1$, $E2$	electric-dipole, electric-quadrupole
EFT	effective field theory
F	Fermi
GT	Gamow-Teller
h.c.	hermitian congugate
HF	Hartree–Fock
IAS	isobaric analogue state
IMME	isobaric-multiplet mass equation
IMSRG	in-medium similarity-renormalization group
INC	Isospin-nonconserving
$M1$	magnetic-dipole
MED	mirror energy difference
N^{3}LO	next-to-next-to-next-to-leading
NN	nucleon–nucleon
rms	root mean square
TED	triplet energy difference
TMBE	two-body matrix element
$V-A$	vector–axial vector
WS	Wood-Saxon
USD	universal sd shell
χEFT	chiral effective field theory
$3N$	three-nucleon

References

1. Heisenberg, W. Über den Bau der Atomkerne. I. *Z. Phys.* **1932**, *77*, 1–11. [CrossRef]
2. Hesenberg, W. On the structure of atomic nuclei. I. In *Nuclear Forces*; Brink, D.M., Ed.; Pergamon Press: Oxford, UK, 1965; p. 214.
3. Wigner, E. On the consequences of the symmetry of the nuclear Hamiltonian on the spectroscopy of nuclei. *Phys. Rev.* **1937**, *51*, 106–119. [CrossRef]
4. Wigner, E. Isotopic spin—A quantum number for nuclei. In *Proceedings of the Robert A. Welch Foundation Conference on Chemical Research*; Milligan, W.O., Ed.; Welch Foundation: Houston, TX, USA, 1957; Volume 1, pp. 67–91.
5. Lam, Y.H.; Blank, B.; Smirnova, N.A.; Antony, M.S.; Bueb, J. The isobaric multiplet mass equation for $A \leq 71$ revisited. *At. Data Nucl. Data Tables* **2013**, *99*, 680–703. [CrossRef]
6. MacCormick, M.; Audi, G. Evaluated experimental isobaric analogue states from $T = 1/2$ to $T = 3$ and associated IMME coefficients. *Nucl. Phys. A* **2014**, *925*, 61–95. [CrossRef]
7. Frank, A.; Jolie, A.; Van Isacker, P. *Symmetries in Atomic Nuclei*; Springer Science+Business Media, LLC: New York, NY, USA, 2009. [CrossRef]
8. Warburton, E.K.; Weneser, J. The role of isospin in electromagnetic transitions. In *Isospin in Nuclear Physics*; Wilkinson, D.H., Ed.; North-Holland Publishing Co.: Amsterdam, The Netherlands, 1969; pp. 152–228.
9. Wilkinson, D.H. (Ed.) *Isospin in Nuclear Physics*; North-Holland Publishing Co.: Amsterdam, The Netherlands, 1969.
10. Harney, H.L.; Richter, A.; Weidenmüller, H.A. Breaking of isospin symmetry in compound-nucleus reactions. *Rev. Mod. Phys.* **1986**, *58*, 607–645. [CrossRef]
11. Fujita, Y.; Rubio, B.; Gelletly, W. Spin–isospin excitations probed by strong, weak and electro-magnetic interactions. *Prog. Part. Nucl. Phys.* **2011**, *66*, 549–606. [CrossRef]
12. Machleidt, R. The meson theory of nuclear forces and nuclear structure. In *Advances in Nuclear Physics. Volume 19*; Negele, J.W., Vogt, E., Eds.; Plenum Press: New York, NY, USA, 1989; Chapter 2. [CrossRef]
13. Epelbaum, E.; Hammer, H.-W. ; Meißner, U.-G. Modern theory of nuclear forces. *Rev. Mod. Phys.* **2009**, *81*, 1773–1825. [CrossRef]
14. Nolen, J.A.; Schiffer, J.P. Coulomb energies. *Ann. Rev. Nucl. Sci.* **1969**, *19*, 471–526. [CrossRef]
15. Ormand, W.E.; Brown, B.A. Empirical isospin-nonconserving Hamiltonians for shell-model calculations. *Nucl. Phys. A* **1989**, *491*, 1–23. [CrossRef]
16. Nakamura, S.; Muto, K. ; Oda, T. Isospin-forbidden beta decays in *ls0d*-shell nuclei. *Nucl. Phys. A* **1994**, *575*, 1–45. [CrossRef]
17. Zuker, A.P.; Lenzi, S.M.; Martinez-Pinedo, G.; Poves, A. Isobaric multiplet yrast energies and isospin nonconserving forces. *Phys. Rev. Lett.* **2002**, *89*, 142502. [CrossRef] [PubMed]

18. Henley, E.M.; Miller, G.A. Meson theory of charge-dependent nuclear forces. In *Mesons in Nuclei. Volume 1*; Rho, M., Wilkinson, D.H., Eds.; North-Holland Publishing Co.: Amsterdam, The Netherlands, 1979; pp. 405–434.

19. Miller, G.A.; Nefkens, B.M.K.; Slaus, I. Charge symmetry, quarks and mesons. *Phys. Rep.* **1990**, *194*, 1–116. [CrossRef]

20. van Kolck, U.L. Soft Physics: Applications of Effective Chiral Lagrangians to Nuclear Physics and Quark Models. Ph.D. Thesis, The University of Texas at Austn, Austin, TX, USA, 1993. Available online: https://www.proquest.com/openview/b885fad2126b5b81a16dca7d226f854a/ (accessed on 7 March 2023).

21. Epelbaum, E. Few-nucleon forces and systems in chiral effective field theory. *Prog. Part. Nucl. Phys.* **2006**, *57*, 654–741. [CrossRef]

22. Machleidt, R.; Entem, D.R. Chiral effective field theory and nuclear forces. *Phys. Rep.* **2011**, *503*, 024001. [CrossRef]

23. Wiringa, R.B.; Pastore, S.; Pieper, S.C.; Miller, G.A. Charge-symmetry breaking forces and isospin mixing in ^{8}Be. *Phys. Rev. C* **2013**, *88*, 044333. [CrossRef]

24. Barrett, B.R.; Navrátil, P.; Vary, J.P. *Ab initio* no core shell model. *Prog. Part. Nucl. Phys.* **2013**, *57*, 654–741. [CrossRef]

25. Maris, P.; Epelbaum, E.; Furnstahl, R.J.; Golak, J.; Hebeler, K.; Hüther, T.; Kamada, H.; Krebs, H.; Meißner, U.-G.; Melendez, J.A.; et al. Light nuclei with semilocal momentum-space regularized chiral interactions up to third order. *Phys. Rev. C* **2021**, *103*, 054001. [CrossRef]

26. Caprio, M.A.; Fasano, P.J.; Maris, P.; McCoy, A.E. Quadrupole moments and proton-neutron structure in *p*-shell mirror nuclei. *Phys. Rev. C* **2021**, *104*, 034319. [CrossRef]

27. Lam, Y.H.; Smirnova, N.A.; Caurier, E. Isospin nonconservation in *sd*-shell nuclei. *Phys. Rev. C* **2013**, *87*, 054304. [CrossRef]

28. Kaneko, K.; Sun, Y.; Mizusaki, T.; Tazaki, S. Variation in displacement energies due to isospin-nonconserving forces. *Phys. Rev. Lett.* **2013**, *110*, 172505. [CrossRef]

29. Kaneko, K.; Sun, Y.; Mizusaki, T.; Tazaki, S. Isospin-nonconserving interaction in the $T = 1$ analogue states of the mass-70 region. *Phys. Rev. C* **2014**, *89*, 031302. [CrossRef]

30. Holt, J.D.; Menendez, J.; Schwenk, A. Three-body forces and proton-rich nuclei. *Phys. Rev. Lett.* **2013**, *110*, 022502. [CrossRef] [PubMed]

31. Bentley, M.; Lenzi, S.M.; Simpson, S.A.; Diget, C.A. Isospin-breaking interactions studied through mirror energy differences. *Phys. Rev. C* **2015**, *92*, 024310. [CrossRef]

32. Lenzi, S.M.; Bentley, M.; Lau, R.; Diget, C.A. Isospin-symmetry breaking corrections for the description of triplet energy differences. *Phys. Rev. C* **2018**, *98*, 054322. [CrossRef]

33. Ormand, W.E.; Brown, B.A.; Hjorth-Jensen, M. Realistic calculations for *c* coefficients of the isobaric mass multiplet equation in $1p0f$ shell nuclei. *Phys. Rev. C* **2017**, *96*, 024323. [CrossRef]

34. Magilligan, A.; Brown, B.A. New isospin-breaking "USD" Hamiltonians for the *sd* shell. *Phys. Rev. C* **2020**, *101*, 064312. [CrossRef]

35. Martin, M.S.; Stroberg, S.R.; Holt, J.D.; Leach, K.G. Testing isospin symmetry breaking in *ab initio* nuclear theory. *Phys. Rev. C* **2021**, *104*, 014324. [CrossRef]

36. Caurier, E.; Navrátil, P.; Ormand, W.E.; Vary, J.P. *Ab initio* shell model for $A = 10$ nuclei. *Phys. Rev. C* **2002**, *66*, 024314. [CrossRef]

37. Michel, N.; Nazarewicz, W.; Płoszajczak, M. Isospin mixing and the continuum coupling in weakly bound nuclei. *Phys. Rev. C* **2010**, *82*, 044315. [CrossRef]

38. Sagawa, H.; Van Giai, N.; Suzuki, T. Effect of isospin mixing on superallowed Fermi *β* decay. *Phys. Rev. C* **1996**, *53*, 2163–2170. [CrossRef]

39. Liang, H.; Van Giai, N.; Meng, J. Isospin corrections for superallowed Fermi *β* decay in self-consistent relativistic random-phase approximation approaches. *Phys. Rev. C* **2009**, *79*, 064316. [CrossRef]

40. Petrovici, A. Isospin-symmetry breaking and shape coexistence in $A \approx 70$ analogs. *Phys. Rev. C* **2015**, *91*, 014302. [CrossRef]

41. Satuła, W.; Dobaczewski, J.; Nazarewicz, W.; Rafalski, M. Microscopic calculations of isospin-breaking corrections to superallowed beta decay. *Phys. Rev. Lett.* **2011**, *106*, 132502. [PubMed]

42. Satula, W.; Dobaczewski, J.; Nazarewicz, W.; Rafalski, M. Isospin-breaking corrections to superallowed Fermi *β* decay in isospin- and angular-momentum-projected nuclear density functional theory. *Phys. Rev. C* **2012**, *86*, 054316. [CrossRef]

43. Satuła, W.; Bączyk, P.; Dobaczewski, J.; Konieczka, M. No-core configuration-interaction model for the isospin- and angular-momentum-projected states. *Phys. Rev. C* **2016**, *94*, 024306. [CrossRef]

44. Bączyk, P.; Dobaczewski, J.; Konieczka, M.; Nakatsukasa, T.; Sato, K.; Satula, W. Isospin-symmetry breaking in masses of $N \approx Z$ nuclei. *Phys. Lett. B* **2018**, *778*, 178–183. [CrossRef]

45. Baczyk, P.; Satula, W.; Dobaczewski, J.; Konieczka, M. Isobaric multiplet mass equation within nuclear density functional theory. *J. Phys. G* **2019**, *46*, 03LT01. [CrossRef]

46. Roca-Maza, X.; Colò, G.; Sagawa, H. Nuclear symmetry energy and the breaking of the isospin symmetry: How do they reconcile with each other? *Phys. Rev. Lett.* **2018**, *120*, 202501. [CrossRef]

47. Naito, T.; Colò, G.; Liang, H.; Roca-Maza, X.; Sagawa, H. Toward *ab initio charge* symmetry breaking in nuclear energy density functionals. *Phys. Rev. C* **2022**, *105*, L021304. [CrossRef]

48. Bertsch, G.F.; Mekjian, A. Isospin impurities in nuclei. *Ann. Rev. Nucl. Sci.* **1972**, *22*, 25–64. [CrossRef]

49. Raman, S.; Walkiewicz, T.A.; Behrens, H. Superallowed $0^+ \rightarrow 0^+$ and isospin-forbidden $J^\pi \rightarrow J^\pi$ Fermi transitions. *At. Data Nucl. Data Tables* **1975**, *16*, 451–494. [CrossRef]

50. Auerbach, N. Coulomb effects in nuclear structure. *Phys. Rep.* **1983**, *98*, 273–341. [CrossRef]

51. Brussaard P.J.; Glaudemans P.W.M. *Shell-Model Applications in Nuclear Spectroscopy*; North-Holland Publishing Co.: Amsterdam, The Netherlands, 1977.
52. Heyde, K.L.G. *The Nuclear Shell Model*; CRC Press/Taylor & Francis Group: Boca Raton, FL, USA, 2004. [CrossRef]
53. Suhonen, J. *From Nucleons to Nucleus*; Springer: Heidelberg/Berlin, Germany, 2007. [CrossRef]
54. Caurier, E.; Martínez-Pinedo, G.; Nowacki, F.; Poves, A.; Zuker, A.P. The shell model as a unified view of nuclear structure. *Rev. Mod. Phys.* **2005**, *77*, 427-488. [CrossRef]
55. Smirnova, N.A. Isospin-symmetry breaking in nuclear structure. *Nuovo Cim. C* **2019**, *42*, 54. [CrossRef]
56. Bertsch, G.F. Role of core polarization in two-body interaction. *Nucl. Phys.* **1965**, *74*, 234–240. [CrossRef]
57. Kuo, T.T.S.; Brown, G.E. Structure of finite nuclei and the free nucleon-nucleon interaction. An application to ^{18}O and ^{18}F. *Nucl. Phys.* **1966**, *85*, 40–86. [CrossRef]
58. Hjorth-Jensen, M.; Kuo, T.T.S.; Osnes, E. Realitic effective interactions for nuclear systems. *Phys. Rep.* **1995**, *261*, 125–270. [CrossRef]
59. Coraggio, A.; Covello, A.; Gargano, A.; Itaco, N.; Kuo, T.T.S. Shell-model calculations and realistic effective interactions. *Prog. Part. Nucl. Phys.* **2009**, *62*, 135–182. [CrossRef]
60. Stroberg, S.R.; Hergert, H.; Bogner, S.; Holt, J.D. Nonempirical interactions for the nuclear shell model: An update. *Ann. Rev. Nucl. Part. Sci.* **2019**, *69*, 307–362. [CrossRef]
61. Poves, A.; Zuker, A.P. Theoretical spectroscopy and the fp shell. *Phys. Rep.* **1981**, *70*, 235–314. [CrossRef]
62. Barrett, B.R. Theoretical approaches to many-body perturbation theory and challenges. *J. Phys. G: Nucl. Part. Phys.* **2005**, *31*, S1349–S1355. [CrossRef]
63. Stroberg, S.R.; Calci, A.; Hergert, H.; Holt, J.D.; Bogner, S.; Roth, R.; Schwenk, A. Nucleus-dependent valence-space approach to nuclear structure. *Phys. Rev. Lett.* **2017**, *118*, 032502. [CrossRef] [PubMed]
64. Dikmen, E.; Lisetskiy, A.F.; Barrett, B.R.; Maris, P.; Shirokov, A.M.; Vary, J.P. *Ab initio* effective interactions for sd-shell valence nucleons. *Phys. Rev. C* **2015**, *91*, 064301. [CrossRef]
65. Smirnova, N.A.; Barrett, B.R.; Kim, Y.; Shin, I.J.; Shirokov, A.M.; Dikmen, E.; Maris, P.; Vary, J.P. Effective interactions in the sd shell. *Phys. Rev. C* **2019**, *100*, 054329. [CrossRef]
66. Jansen, G.R.; Engel, J.; Hagen, G.; Navrátil, P.; Signoracci, A. *Ab initio* coupled-cluster effective interactions for the shell model: Application to neutron-rich oxygen and carbon isotopes. *Phys. Rev. Lett.* **2014**, *113*, 142502. [CrossRef]
67. Jansen, G.R.; Schuster, M.D.; Signoracci, A.; Hagen, G.; Navrátil, P. Open sd-shell nuclei from first principles. *Phys. Rev. C* **2016**, *94*, 011301. [CrossRef]
68. Sun, Z.H.; Morris, T.D.; Hagen, G.; Jansen, G.R.; Papenbrock, T. Shell-model coupled-cluster method for open-shell nuclei. *Phys. Rev. C* **2018**, *98*, 054320. [CrossRef]
69. Fukui, T.; De Angelis, L.; Ma, Y.Z.; Coraggio, A.; Gargano, A.; Itaco, N.; Xu, F. Realistic shell-model calculations for p-shell nuclei including contributions of a chiral three-body force. *Phys. Rev. C* **2018**, *98*, 044305. [CrossRef]
70. Ma, Y.Z.; Coraggio, A.; De Angelis, L.; Fukui, T.; Gargano, A.; Itaco, N.; Xu, F. Contribution of chiral three-body forces to the monopole component of the effective shell-model Hamiltonian. *Phys. Rev. C* **2019**, *100*, 034324. [CrossRef]
71. Cohen, S.; Kurath, D. Effective interactions for the 1p shell. *Nucl. Phys.* **1965**, *73*, 1–24. [CrossRef]
72. Wildenthal, B.H. Empirical strengths of spin operators in nuclei. *Prog. Part. Nucl. Phys.* **1984**, *11*, 5–51. . [CrossRef]
73. Richter, W.A.; Brown, B.A. New "USD" Hamiltonians for the sd shell. *Phys. Rev. C* **2006**, *85*, 045806. [CrossRef]
74. Poves, A.; Sanchez-Solano, J.; Caurier, E.; Nowacki, F. Shell model study of the isobaric chains $A = 50$, $A = 51$ and $A = 52$. *Nucl. Phys. A* **2001**, *694*, 157–198. [CrossRef]
75. Honma, M.; Otsuka, T.; Brown, B.A.; Mizusaki, T. New effective interaction for pf-shell nuclei and its implications for the stability of the $N = Z = 28$ closed core. *Phys. Rev. C* **2004**, *69*, 034335. [CrossRef]
76. Zhang, Y.H.; Zhang, P.; Zhou, X.H.; Wang, M.; Litvinov, Yu.A.; Xu, H.S.; Xu, X.; Shuai, P.; Lam, Y.H.; Chen, R.J.; et al. Isochronous mass measurements of $T\_z = -1$ fp-shell nuclei from projectile fragmentation of ^{58}Ni. *Phys. Rev. C* **2018**, *98*, 014319. [CrossRef]
77. Brown, B.A.; Rae, W.D.M. The shell-model code NuShellX. *Nucl. Data Sheets* **2014**, *120*, 115–118. [CrossRef]
78. Jänecke, J. Vector and tensor Coulomb energies. *Phys. Rev.* **1966**, *147*, 735–742. [CrossRef]
79. Klochko, O.; Smirnova, N.A. Isobaric-multiplet mass equation in a macroscopic-microscopic approach. *Phys. Rev. C* **2021**, *103*, 024316. [CrossRef]
80. Bentley, M.A.; Lenzi, S.M. Coulomb energy differences between high-spin states in isobaric multiplets. *Prog. Part. Nucl. Phys.* **2007**, *59*, 497–561. [CrossRef]
81. Warner, D.D.; Van Isacker, P.; Bentley, M.A. The role of isospin symmetry in collective nuclear structure. *Nat. Phys.* **2006**, *2*, 311–318. [CrossRef]
82. Bentley, M.A. Excited states in isobaric multiplets—Experimental advances and the shell-model approach. *Physics* **2022**, *4*, 995–1011. [CrossRef]
83. Lenzi, S.M.; Poves, A.; Macchiavelli, A.O. Isospin symmetry breaking in the mirror pair ^{73}Sr - ^{73}Br. *Phys. Rev. C* **2020**, *102*, 031302. [CrossRef]
84. Boso, A.; Lenzi, S.M.; Recchia, F.; Bonnard, J.; Zuker, A.P.; Aydin, S.; Bentley, M.A.; Cederwall, B.; Clement, E.; de France, G.; et al. Neutron skin effects in mirror energy differences: The case of ^{23}Mg–^{23}Na. *Phys. Rev. Lett.* **2018**, *121*, 032502. [CrossRef] [PubMed]
85. Thomas, R.G. An analysis of the energy levels of the mirror nuclei, C^{13} and N^{13}. *Phys. Rev.* **1952**, *88*, 1109–1125. [CrossRef]

86. Ehrman, J.B. On the displacement of corresponding energy levels of C^{13} and N^{13}. *Phys. Rev.* **1951**, *81*, 412–416. [CrossRef]

87. Longfellow, B.; Gade, A.; Brown, B.A.; Richter, W.A.; Bazin, D.; Bender, P.C.; Bowry, M.; Elman, B.; Lunderberg, B.E.; Weisshaar, D.; et al. Measurement of key resonances for the ^{24}Al$(p, \gamma)^{25}$Si reaction rate using in-beam γ-ray spectroscopy. *Phys. Rev. C* **2018**, *97*, 054307. [CrossRef]

88. Cenxi, Y.; Qi, C.; Xu, F.; Suzuki, T.; Otsuka, T. Mirror energy difference and the structure of loosely bound proton-rich nuclei around $A = 20$. *Phys. Rev. C* **2014**, *89*, 044327. [CrossRef]

89. Pape, A.; Antony, M.S. Masses of proton-rich $T_z < 0$ nuclei with isobaric mass equation. *At. Data Nucl. Data Tables* **1988**, *39*, 201–203. [CrossRef]

90. Brown, B.A. Diproton decay of nuclei on the proton drip line. *Phys. Rev. C* **1991**, *43*, 1513(R)–1517(R). [CrossRef]

91. Ormand, W.E. Mapping the proton drip line up to $A = 70$. *Phys. Rev. C* **1997**, *55*, 2407–2417. [CrossRef]

92. Brown, B.A.; Clement, R.R.C.; Schatz, H.; Volya, A.; Richter, W.A. Proton drip-line calculations and the rp process. *Phys. Rev. C* **2002**, *65*, 045802. [CrossRef]

93. Richter, W.A.; Brown, B.A.; Signoracci, A.; Wiescher, M. Properties of ^{26}Mg and ^{26}Si in the *sd* shell model and the determination of the ^{26}Al$(p, \gamma)^{26}$Si reaction rate. *Phys. Rev. C* **2011**, *83*, 065803. [CrossRef]

94. Benenson, W.; Kashy, E. Isobaric quartests in nuclei. *Rev. Mod. Phys.* **1979**, *51*, 527–540. [CrossRef]

95. Zhang, Y.H.; Xu, H.S.; Litvinov, Yu.A.; Tu, X.L.; Yan, X.L.; Typel, S.; Blaum, K.; Wang, M.; Zhou, X.H.; Sun, Y.; et al. Mass measurements of the neutron-deficient ^{41}Ti, ^{45}Cr, ^{49}Fe, and ^{53}Ni nuclides: First test of the isobaric multiplet mass equation in fp-shell nuclei. *Phys. Rev. Lett* **2012**, *109*, 102501. [CrossRef] [PubMed]

96. Brodeur, M.; Kwiatkowski, A.A.; Drozdowski, O.M.; Andreoiu, C.; Burdette, D.; Chaudhuri, A.; Chowdhury, U.; Gallant, A.T.; Grossheim, A.; Gwinner, G.; et al. Precision mass measurements of magnesium isotopes and implications for the validity of the isobaric mass multiplet equation. *Phys. Rev. C* **2017**, *96*, 034316. [CrossRef]

97. Bertsch, G.F.; Kahana, S. T_z^3 term in the isobaric multiplet equation. *Phys. Lett. B* **1970**, *33*, 193–194. [CrossRef]

98. Signoracci, A.; Brown, B.A. Effects of isospin mixing in the $A = 32$ quintet. *Phys. Rev. C* **2011**, *84*, 031301. [CrossRef]

99. Kamil, M.; Triambak, S.; Magilligan, A.; García, A.; Brown, B.A.; Adsley, P.; Bildstein, V.; Burbadge, C.; Diaz Varela, A.; Faestermann, T.; et al. Isospin mixing and the cubic isobaric multiplet mass equation in the lowest $T = 2$, $A = 32$ quintet. *Phys. Rev. C* **2022**, *104*, L061303. [CrossRef]

100. Barker, F.C. Intermediate coupling shell-model calculations for light nuclei. *Nucl. Phys.* **1966**, *83*, 418–448. [CrossRef]

101. Smirnova, N.A.; Blank, B.; Brown, B.A.; Richter, W.A.; Benouaret, N.; Lam, Y.H. Theoretical analysis of isospin mixing with the β decay of ^{56}Zn. *Phys. Rev. C* **2016**, *93*, 044305. [CrossRef]

102. Hoyle, C.D.; Adelberger, E.G.; Blair, J.S.; Snover, K.A.; Swanson, H.E.; Von Lintig, R.D. Isospin mixing in ^{24}Mg. *Phys. Rev. C* **1983**, *27*, 1244–1259. [CrossRef]

103. Orrigo, S.; Rubio, B.; Fujita, Y.; Blank, B.; Gelletly, W.; Agramunt, J.; Algora, A.; Ascher, P.; Bilgier, B.; Cáceres, L.; et al. Observation of the β-delayed γ-proton decay of ^{56}Zn and its impact on the Gamow-Teller strength evaluation. *Phys. Rev. Lett.* **2014**, *112*, 222501. [CrossRef] [PubMed]

104. Hagberg, E.; Koslowsky, V.T.; Hardy, J.C.; Towner, I.S.; Hykawy, J.G.; Savard, G.; Shinozuka, T. Tests of isospin mixing corrections in superallowed $0^+ \rightarrow 0^+$ β decays. *Phys. Rev. Lett* **1994**, *73*, 396–399. [CrossRef] [PubMed]

105. MacLean, A.D.; Laffoley, A.T.; Svensson, C.E.; Ball, G.C.; Leslie, J.T.; Andreoiu, C.; Babu, A.; Bhattacharjee, S.S.; Bidaman, H.; Bildstein, V.; et al. High-precision branching ratio measurement and spin assignment implications for ^{62}Ga superallowed β decay. *Phys. Rev. C* **2020**, *102*, 054325. [CrossRef]

106. Schuurmans, P.; Camps, J.; Phalet, T.; Severijns, N.; Vereecke, B.; Versyck, S. Isospin mixing in the ground state of ^{52}Mn. *Nucl. Phys. A* **2000**, *672*, 89–98. [CrossRef]

107. Severijns, N.; Vénos, D.; Schuurmans, P.; Phalet, T.; Honusek, M.; Srnka, D.; Vereecke, B.; Versyck, S.; Zákoucký, D.; Köster, U.; et al. Isospin mixing in the $T = 5/2$ ground state of ^{71}As. *Phys. Rev. C* **2005**, *71*, 064310. [CrossRef]

108. Farnea, E.; de Angelis, G.; Gadea, A.; Bizzeti, P.G.; Dewald, A.; Eberth, J.; Algora, A.; Axiotis, M.; Bazzacco, D.; Bizzeti-Sona, A.M.; et al. Isospin mixing in the $N = Z$ nucleus ^{64}Ge. *Phys. Lett. B* **2004**, *551*, 56–62. [CrossRef]

109. Bizzeti, P.G.; de Angelis, G.; Lenzi, S.M.; Orlandi, R. Isospin symmetry violation in mirror $E1$ transitions: Coherent contributions from the giant isovector monopole resonance in the ^{67}As–^{67}Se doublet. *Phys. Rev. C* **2012**, *86*, 044311. [CrossRef]

110. Lisetskiy, A.F.; Schmidt, A.; Schneider, I.; Friessner, C.; Pietralla, N.; von Brentano, P. Isospin mixing between low-lying states of the odd-odd $N = Z$ nucleus ^{54}Co. *Phys. Rev. Lett.* **2002**, *89*, 012502. [CrossRef]

111. Prados-Estevez, F.M.; Bruce, A.M.; Taylor, M.J.; Amro, H.; Beausang, C.W.; Casten, R.F.; Ressler, J.J.; Barton, C.J.; Chandler, C.; Hammond, G. Isospin purity of $T = 1$ states in the $A = 38$ nuclei studied via lifetime measurements in ^{38}K. *Phys. Rev. C* **2007**, *75*, 014309. [CrossRef]

112. Giles, M.M.; Nara Singh, B.S.; Barber, L.; Cullen, D.M.; Mallaburn, M.J.; Beckers, M.; Blazhev, A.; Braunroth, T.; Dewald, A.; Fransen, C.; et al. Probing isospin symmetry in the (^{50}Fe, ^{50}Mn, ^{50}Cr) isobaric triplet via electromagnetic transition rates. *Phys. Rev. C* **2019**, *99*, 044317. [CrossRef]

113. Bizzeti, P.G.; Bizzeti-Sona, A.M.; Cambi, A.; Mandò, M.; Maurenzig, P.R.; Signorini, C. Strength of analogue $E2$ transitions in ^{30}Si and ^{30}P. *Lett. Nuovo Cim.* **1969**, *16*, 775. [CrossRef]

114. Ekman, J.; Rudolph, D.; Fahlander, C.; Zuker, A.P.; Bentley, M.A.; Lenzi, S.M.; Andreoiu, C.; Axiotis, M.; de Angelis, G.; Farnea, E.; et al. Unusual isospin-breaking and isospin-mixing effects in the $A = 35$ mirror nuclei. *Phys. Rev. Lett.* **2004**, *92*, 132502. [CrossRef] [PubMed]

115. Pattabiraman, N.S.; Jenkins, D.G.; Bentley, M.A.; Wadsworth, R.; Lister, C.J.; Carpenter, M.P.; Janssens, R.V.F.; Khoo, T.L.; Lauritsen, T.; Seweryniak, D.; et al. Analog $E1$ transitions and isospin mixing. *Phys. Rev. C* **2008**, *78*, 024301. [CrossRef]

116. von Neumann-Cosel, P.; Gräf, H.-D.; Krämer, U.; Richter, A.; Spamer, E. Electroexcitation of isoscalar and isovector magnetic dipole transitions in ^{12}C and isospin mixing. *Nucl. Phys. A* **2000**, *669*, 3–13. [CrossRef]

117. Corsi, A.; Wieland, O.; Barlini, S.; Bracco, A.; Camera, F.; Kravchuk, V.L.; Baiocco, G.; Bardelli, L.; Benzoni, G.; Bini, M.; et al. Measurement of isospin mixing at a finite temperature in ^{80}Zr via giant dipole resonance decay. *Phys. Rev. C* **2011**, *84*, 041304(R). [CrossRef]

118. Ceruti, S.; Camera, F.; Bracco, A.; Avigo, R.; Benzoni, G.; Blasi, N.; Bocchi, G.; Bottoni, S.; Brambilla, S.; Crespi, F.C.L.; et al. Isospin mixing in ^{80}Zr: From finite to zero temperature. *Phys. Rev. Lett.* **2016**, *115*, 222502. [CrossRef]

119. Gosta, G.; Mentana, A.; Camera, F.; Bracco, A.; Ceruti, S.; Benzoni, G.; Blasi, N.; Brambilla, S.; Capra, S.; Crespi, F.C.L.; et al. Probing isospin mixing with the giant dipole resonance in the ^{60}Zn compound nucleus. *Phys. Rev. C* **2021**, *103*, L041302. [CrossRef]

120. Brown, B.A. Isospin-forbidden β-delayed proton emission. *Phys. Rev. Lett.* **1990**, *65*, 2753–2756. [CrossRef]

121. Dossat, C.; Adimi, F.; Aksouh, F.; Becker, F.; Bey, A.; Blank, B.; Borcea, C.; Borcea, R.; Boston, A.; Caamano, M.; et al. The decay of proton-rich nuclei in the mass $A = 36 - 56$ region. *Nucl. Phys. A* **2005**, *792*, 18–86. [CrossRef]

122. Blank, B.; Borge, M.J.G. Nuclear structure at the proton drip line: Advances with nuclear decay studies. *Prog. Part. Nucl. Phys.* **2008**, *60*, 403–483. [CrossRef]

123. Ormand, W.E.; Brown, B.A. Isospin-forbidden proton and neutron emission in 1s-0d shell nuclei. *Phys. Lett. B* **1986**, *174*, 128–132. [CrossRef]

124. Smirnova, N.A.; Blank, B.; Richter, W.A.; Brown, B.A.; Benouaret, N.; Lam, Y.H. Isospin mixing from β-delayed proton emission. *Phys. Rev. C* **2017**, *95*, 054301. [CrossRef]

125. Saxena, M.; Ong, W.-J.; Meisel, A.; Hoff, D.E.M.; Smirnova, N.; Bender, P.C.; Burcher, S.P.; Carpenter, M.P.; Carroll, J.J.; Chester, A.; et al. ^{57}Zn β-delayed proton emission establishes the ^{56}Ni rp-process waiting point bypass. *Phys. Lett. B* **2022**, *829*, 137059. [CrossRef]

126. Towner, I.S.; Hardy, J.C. Currents and their couplings in the weak sector of the Standard Model. In *Symmetries and Fundamental Interactions in Nuclei*; Henley, E.M., Haxton, W.C., Eds.; World Scientific: Singapore, 1995; pp. 183–249. [CrossRef]

127. Severijns, N.; Beck, M.; Naviliat-Cuncic, O. Tests of the standard electroweak model in nuclear beta decay. *Rev. Mod. Phys.* **2006**, *78*, 991–1040. [CrossRef]

128. González-Alonso, M.; Naviliat-Cuncic, O.; Severijns, N. New physics searches in nuclear and neutron β-decay. *Prog. Part. Nucl. Phys.* **2019**, *104*, 165–223. [CrossRef]

129. Towner, I.S.; Hardy, J.C. The evaluation of V_{ud} and its impact on the unitarity of the Cabibbo–Kobayashi– Maskawa quark-mixing matrix. *Rep. Prog. Phys.* **2010**, *73*, 046301. [CrossRef]

130. Hardy, J.C.; Towner, I.S. Superallowed $0^+ \rightarrow 0^+$ nuclear β decays: 2020 critical survey, with implications for V_{ud} and CKM unitarity. *Phys. Rev.* **2020**, *102*, 045501. [CrossRef]

131. Seng, C.-Y.; Gorchtein, M.; Patel, H.H.; Ramsey-Musolf, M.J. Reduced Hadronic Uncertainty in the Determination of V_{ud}. *Phys. Rev. Lett.* **2018**, *121*, 241804. [CrossRef]

132. Ormand, W.E.; Brown, B.A. Isospin-mixing corrections for fp-shell Fermi transitions. *Phys. Rev. C* **1995**, *52*, 2455–2460. [CrossRef]

133. Damgaard, J. Corrections to the ft-values of $0^+ \rightarrow 0^+$ superallowed β-decays. *Nucl. Phys. A* **1969**, *130*, 233–240. [CrossRef]

134. Auerbach, N. Coulomb corrections to superallowed β decay in nuclei. *Phys. Rev. C* **2009**, *79*, 035502. [CrossRef]

135. Xayavong, L.; Smirnova, N.A. Radial overlap correction to superallowed $0^+ \rightarrow 0^+$ β decay reexamined. *Phys. Rev. C* **2018**, *97*, 024324. [CrossRef]

136. Miller, G.A.; Schwenk, A. Isospin-symmetry-breaking corrections to superallowed Fermi β decay. Formalism and schematic models. *Phys. Rev. C* **2008**, *78*, 035501. [CrossRef]

137. Miller, G.A.; Schwenk, A. Isospin-symmetry-breaking corrections to superallowed Fermi β decay: Radial excitations. *Phys. Rev. C* **2009**, *80*, 064319. [CrossRef]

138. Towner, I.S.; Hardy, J.C. Improved calculations of isospin-symmetry breaking corrections to superallowed Fermi β decay. *Phys. Rev. C* **2008**, *77*, 025501. [CrossRef]

139. Hardy, J.C.; Towner, I.S. Superallowed $0^+ \rightarrow 0^+$ nuclear β decays: 2014 critical survey, with precise results for V_{ud} and CKM unitarity. *Phys. Rev.* **2015**, *91*, 025501. [CrossRef]

140. Ormand, W.E.; Brown, B.A. Corrections to the Fermi matrix element for superallowed β decay. *Phys. Rev. Lett.* **1989**, *62*, 866–869. [CrossRef]

141. Towner, I.S.; Hardy, J.C. Comparative tests of isospin-symmetry breaking corrections to superallowed $0^+ \rightarrow 0^+$ nuclear β decay. *Phys. Rev. C* **2010**, *82*, 065501. [CrossRef]

142. Ormand, W.E.; Brown, B.A. Calculated isospin-mixing corrections to Fermi β-decays in 1s0d-shell nuclei with emphasis on $A = 34$. *Nucl. Phys. A* **1985**, *440*, 274–300. [CrossRef]

143. Xayavong, L.; Smirnova, N.; Bender, M.; Bennaceur, K. Shell-model calculation of isospin-symmetry breaking correction to super-allowed Fermi beta decay. *Acta Phys. Pol. B. Proc. Supp.* **2017**, *10*, 285–290. [CrossRef]

144. Xayavong, L.; Smirnova, N.A. Radial overlap correction to superallowed $0^+ \to 0^+$ nuclear β decays using the shell model with Hartree-Fock radial wave functions. *Phys. Rev. C* **2022**, *105*, 044308. [CrossRef]

145. Naviliat-Cuncic, O.; Severijns, N. Test of the conserved vector current hypothesis in $T = 1/2$ mirror transitions and new determination of V_{ud}. *Phys. Rev. Lett.* **2009**, *102*, 142302. [CrossRef] [PubMed]

146. Towner, I.S. Mirror asymmetry in allowed Gamow-Teller β-decay. *Nucl. Phys. A* **1973**, *216*, 589–602. [CrossRef]

147. Smirnova, N.A.; Volpe, M.C. On the asymmetry of Gamow-Teller β-decay rates in mirror nuclei in relation with second-class currents. *Nucl. Phys. A* **2003**, *714*, 441–462. [CrossRef]

148. Grenacs, L. Induced weak currents in nuclei. *Ann. Rev. Nucl. Part. Sci.* **1985**, *35*, 455–499. [CrossRef]

149. Minamisono, K.; Nagatomo, T.; Matsuta, K.; Levy, C.D.P.; Tagishi, Y.; Ogura, M.; Yamaguchi, M.; Ota, H.; Behr, J.A.; Jackson, K.P.; et al. Low-energy test of second-class current in β decays of spin-aligned ^{20}F and ^{20}Na. *Phys. Rev. C* **2011**, *84*, 055501. [CrossRef]

150. Langanke, K.; Martinez-Pinedo, G. Nuclear weak-interaction processes in stars. *Rev. Mod. Phys.* **2003**, *75*, 812–862. [CrossRef]

151. Jose, J.; Hernanz, M.; Iliadis, C. Nucleosynthesis in classical novae. *Nucl. Phys. A* **2006**, *777*, 550–578. [CrossRef]

152. Wallace, R.K.; Woosley, S.E. Explosive hydrogen burning. *Astrophys. J. Supp. Ser.* **1981**, *45*, 389–420. [CrossRef]

153. Schatz, H.; Aprahamian, A.; Görres, J.; Wiescher, M.; Rauscher, T.; Rembges, J.F.; Thielemann, F.K.; Pfeiffer, B.; Möller, P.; Kratz, K.-L.; et al. rp-process nucleosynthesis at extreme temperature and density conditions. *Phys. Rep.* **1998**, *294*, 167–263. [CrossRef]

154. Fowler, W.A.; Hoyle, F. Neutrino processes and pair formation in massive stars and supernovae. *Astrophys. J. Supp.* **1964**, *9*, 201–319. [CrossRef]

155. Herndl, H.; Görres, J.; Wiescher, M.; Brown, B.A.; Van Wormer, L. Proton capture reaction rates in the *rp* process. *Phys. Rev. C* **1995**, *52*, 1078–1094. [CrossRef] [PubMed]

156. Fisker, J.L.; Barnard, V.; Görres, J.; Langanke, K.; Martinez-Pinedo, G.; Wiescher, M. Shell-model based reaction rates for *rp*-process nuclei in the mass range $A = 44 - 63$. *At. Data Nucl. Data Tables* **2001**, *79*, 241–292. [CrossRef]

157. Richter, W.A.; Brown, B.A. Shell-model studies of the *rp* reaction ^{35}Ar$(p, \gamma)^{36}$K. *Phys. Rev. C* **2012**, *85*, 045806. [CrossRef]

158. Lam, Y.H.; Herger, A.; Lu, N.; Jacobs, A.M.; Smirnova, N.A.; Kurtukian-Nieto, T.; Johnston, T.; Kubono, S. The regulated NiCu cycles with the new ^{57}Cu$(p, \gamma)^{58}$Zn reaction rate and its influence on type I X-ray bursts: The GS 1826-24 clocked burster. *Astrophys. J.* **2022**, *929*, 73–88. [CrossRef]

159. Brown, B.A.; Richter, W.A.; Wrede, C. Shell-model studies of the astrophysical rapid-proton-capture reaction ^{30}P$(p, \gamma)^{31}$S. *Phys. Rev. C* **2014**, *89*, 062801. [CrossRef]

160. Richter, W.A.; Brown, B.A.; Longland, R.; Wrede, C.; Denissenkov, P.; Fry, C.; Herwig, F.; Kurtulgil, D.; Pignatari, M.; Reifarth, R. Shell-model studies of the astrophysical *rp*-process reactions ^{34}S$(p, \gamma)^{35}$Cl and ^{34g,m}Cl$(p, \gamma)^{35}$Ar. *Phys. Rev. C* **2020**, *102*, 025801. [CrossRef]